Cerebral Cortex, 2016, 1–16

doi: 10.1093/cercor/bhw065
Original Article

ORIGINAL ARTICLE

The Right Dorsal Premotor Mosaic: Organization, Functions, and Connectivity

Sarah Genon[1,2], Hai Li[5,6], Lingzhong Fan[5,6], Veronika I. Müller[1,2], Edna C. Cieslik[1,2], Felix Hoffstaedter[1], Andrew T. Reid[1], Robert Langner[1,2], Christian Grefkes[1,4], Peter T. Fox[3], Susanne Moebus[8], Svenja Caspers[1], Katrin Amunts[1], Tianzi Jiang[5,6,7] and Simon B. Eickhoff[1,2]

[1]Institute of Neuroscience and Medicine (INM-1, INM-3), Research Centre Jülich, Jülich, Germany, [2]Institute of Clinical Neuroscience and Medical Psychology, Heinrich Heine University, Düsseldorf, Germany, [3]Research Imaging Institute, University of Texas Health Science Center at San Antonio, TX, USA, [4]Department of Neurology, Cologne University Hospital, Cologne, Germany, [5]Brainnetome Center, Institute of Automation and, [6]National Laboratory of Pattern Recognition, Institute of Automation, Chinese Academy of Sciences, Beijing 100190, China, [7]Key Laboratory for NeuroInformation of the Ministry of Education, School of Life Science and Technology, University of Electronic Science and Technology of China, Chengdu 625014, China and [8]Centre for Urban Epidemiology (CUE), Universitätsklinikum Essen, University of Duisburg-Essen, Essen, Germany

Address correspondence to Simon B. Eickhoff, Institut für Neurowissenschaften und Medizin (INM-1), Forschungszentrum Jülich GmbH, D-52425 Jülich, Germany. Email: s.eickhoff@fz-juelich.de

Abstract

The right dorsal premotor cortex (PMd) of humans has been reported to be involved in a broad range of motor and cognitive functions. We explored the basis of this behavioral heterogeneity by performing a connectivity-based parcellation using meta-analytic approach applied to PMd coactivations. We compared our connectivity-based parcellation result with parcellations obtained through resting-state functional connectivity and probabilistic diffusion tractography. Functional connectivity profiles and behavioral decoding of the resulting PMd subregions allowed characterizing their respective behavior profile. These procedures divided the right PMd into 5 distinct subregions that formed a cognitive-motor gradient along a rostro-caudal axis. In particular, we found 1) a rostral subregion functionally connected with prefrontal cortex, which likely supports high-level cognitive processes, such as working memory, 2) a central subregion showing a mixed behavioral profile and functional connectivity to parietal regions of the dorsal attention network, and 3) a caudal subregion closely integrated with the motor system. Additionally, we found 4) a dorsal subregion, preferentially related to hand movements and connected to both cognitive and motor regions, and 5) a ventral subregion, whose functional profile fits the concept of an eye movement-related field. In conclusion, right PMd may be considered a functional mosaic formed by 5 subregions.

Key words: activation likelihood estimation, clustering, functional connectivity, parcellation, premotor cortex

Introduction

The premotor cortex (PM) has been defined as a distinct cortical region within the frontal agranular cortex (Wise 1985). The PM is located in the lateral portion of Brodmann's area 6 (BA; Brodmann 1909) on the precentral gyrus, just rostral to the primary motor cortex (M1, BA 4/Area 4; Geyer et al. 2000). However, the

PM is not necessarily equivalent to BA 6, since the region defined as the PM is based on functional criteria, whereas BA 6 is identified by cytoarchitectonic criteria (Brodmann 1909; Geyer et al. 2000). In nonhuman primates, the PM has been anatomically subdivided into a dorsal part (PMd) and a ventral part (PMv) (for a review, see Rizzolatti et al. 1998). In primates, the PMd has been further divided into rostral and caudal subregions based on differences in connectivity (Abe and Hanakawa 2009) and histology (i.e., cytoarchitecture and cytochrome C staining). The rostral subregion, termed F7 (Matelli et al. 1985, 1991), is mainly connected to prefrontal regions, while the caudal subregion, termed F2 (Matelli et al 1991) is connected to the primary motor cortex and spinal cord (Boussaoud et al. 1995; Rizzolatti and Luppino 2001).

The dorso-ventral distinction in nonhuman primates shows correspondence with the subdivision of the human PM into PMd and PMv based on structural connectivity (Tomassini et al. 2007). A broad range of motor and cognitive functions, such as movement preparation, action selection, motor learning, goal salience maintenance, visuospatial imagery, visual attention, and working memory, have been ascribed to the PMd in humans (for reviews, see Boussaoud 2001; Schubotz and von Cramon 2003; Chouinard and Paus 2006; Hoshi and Tanji 2007; Abe and Hanakawa 2009; Kantak et al. 2012; Hoshi 2013). In conjunction with previously identified PMd subregions in nonhuman primates (i.e., F2, F7), such behavioral heterogeneity suggests that the human PMd may not be a uniform region, but rather one comprised several distinct subdivisions with specialized function and connectivity.

Several studies have suggested a rostro-caudal organization corresponding to a cognitive-motor gradient within the frontal regions including the PMd (Yeo et al. 2011; Choi et al. 2012; Orban et al. 2014). Furthermore, several fMRI experiments have been performed to disentangle PMd activity related to cognitive versus motor processing, or hand versus eye movements by contrasting experimental conditions in rather small samples of subjects (Hanakawa et al. 2002; Amiez et al. 2006). Finally, ~~a~~ study has suggested a ventrodorsal organization within the superior part of precentral gyrus based on structural connectivity (Schubotz et al. 2010). However, neither these putative anatomical gradients nor their corresponding behavioural and functional attributes have been directly investigated in the PMd, ~~that is,~~ using a quantitative data-driven approach. Furthermore, to date, no study has examined the connectivity profile of distinct modules within the PMd in humans at rest or challenged with a wide range of task demands.

Using a model-free, multimodal, connectivity-based approach, we sought in the current study to provide a robust, data-driven subdivision of the right PMd, as well as a meta-analytic functional characterization of the resulting subdivisions. Our work may thus provide independent support for the idea of a rostro-caudal organization of the PMd, with rostral parts more strongly associated with cognitive functions, and caudal regions with motor functions and/or for the hypothesis of a ventrodorsal distinction. Our objective was to integrate previous work and hypotheses on the PMd. To best incorporate the findings of previous research lines, we opted for a broad definition of the right PMd, ensuring a maximal coverage of previous activations attributed to this region. Importantly, the issue of the functional heterogeneity of the PMd is further complicated by indirect evidence of functional hemispheric differences (Smith and Jonides 1999; Schubotz and von Cramon 2003), which might be based on differential subdivisions within the right and left PMd. Therefore, in the present study, we focused on the right PMd, while the organization of the left PMd will be addressed in a future study.

We performed connectivity-based parcellation (CBP) based on each voxel's co-activation pattern across a wide range of active tasks (MACM-CBP; Eickhoff et al. 2011). Our objective was not so much to define a rigid set of borders for subregions within the right PMd, but rather to provide an integrative guide of the topographical organization of this region. Accordingly, to ensure that the resulting general topographical pattern was not an artifact of the CBP modality, we performed additional CBP analyses based on the structural connectivity profile of the voxels, as measured by probabilistic diffusion tractography (PDT-CBP; Behrens et al. 2003; Johansen-Berg et al. 2004), and the functional connectivity profile, as measured during the resting state fMRI (RSFC-CBP). We next characterized the functional connectivity profile of the clusters obtained by MACM-CBP by combining resting-state functional connectivity (RSFC) analysis and MACM. Finally, quantitative functional decoding (Amft et al. 2014; Nickl-Jockschat et al. 2014) was performed to robustly characterize the profile of behavioral functions associated with each cluster obtained by MACM-CBP.

Methods

Volume of Interest

In the absence of precise landmarks of the borders of PMd, we based our volume of interest (VOI) definition on several meta-analyses that localized functions commonly attributed to the PMd. Our VOI was defined by merging PMd activation sites from published meta-analyses on action observation (Caspers et al. 2010), motor learning (Hardwick et al. 2013), movement perception (Grosbras et al. 2012), sustained attention (Langner and Eickhoff 2013), and working memory (Rottschy et al. 2012) using an or combination. The ensuing VOI was symmetrized to yield left and right PMd VOIs. Some activation clusters provided by the meta-analyses to some extend overlapped with primary motor cortex (M1) and primary somatosensory cortex (S1). These areas were excluded based on their cytoarchitectonic definition (~~BA~~4a, 4p 3a, 3b, 1, 2) by using the SPM Anatomy Toolbox (Eickhoff et al. 2005). Thus, this procedure ensures that our VOI does not overlap with primary motor cortex on the caudal border as illustrated in Figure 1. In contrast and importantly, our VOI was not restricted to Area 6 on the rostral border.

Finally, white matter voxels were removed from VOI based on the International Consortium on Brain Mapping (ICBM) tissue probability maps (Mazziotta et al. 2001). This procedure yielded a

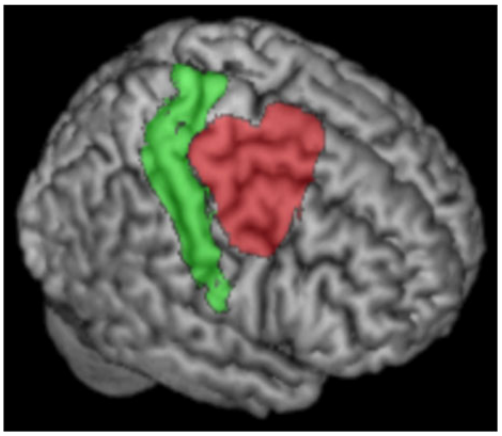

Figure 1. VOI definition. Rendering of sensorimotor areas (areas 1, 2, 3, and 4; green) according to cytoarchitecture (Geyer et al. 1996, 1999, available in the SPM anatomy toolbox) and our PMd VOI (red) in the right hemisphere.

right and a left PMd VOI, comprising 4143 voxels each (voxels size = 1 × 1 × 1) whose inferior and caudal borders are in agreement with previous definition of the PMd (see Supplementary Methods I.1.). The following parcellation procedure was focused on the right PMd VOI.

Connectivity-Based Parcellation

We first performed CBP based on the co-activation profiles of our VOI's voxels by using MACM. The most stable cluster solution (k solution) was chosen based on several criteria in a data-driven approach. To ensure that the revealed topographical organization was not an artifact of our methods based on activation data (cf. discussion), we then searched for a similar k solution based on the structural connectivity profiles of the voxels by using CBP based on PDT (PDT-CBP) and based on the unconstrained functional connectivity profiles of the voxels by using CBP based on RSFC (RSFC-CBP).

Parcellation Based on Co-activation (MACM-CBP). *Meta-Analytic Connectivity Modeling*. Whole-brain co-activation patterns for each voxel within the right PMd were determined by using the BrainMap database (see Supplementary Methods I.2. for a description of the criteria of inclusion of experiments). The experiments associated with each seed voxel were then defined by activation at, or in the immediate vicinity of, this particular voxel. This was performed by calculating the Euclidean distances between a given seed voxel and the individual foci of all experiments. Based on these distances, the extent of a spatial filter was systematically varied from including the closest 20 to 200 experiments in steps of 5. That is, we selected the 20, 25, 30, 35, . . . , 200 experiments reporting activation closest to a given seed voxel. Combining the different filter sizes allowed generating a highly robust co-activation map for every seed voxel independently of subjective choices about the number of associated experiments. This procedure, hence, provided a reliable basis for MACM-CBP, as shown in previous studies (Cieslik et al. 2013; Clos et al. 2013).

The brain-wide co-activation profile for each seed voxel given each of the 37 filter sizes was then computed by a meta-analysis over the associated experiments. This meta-analysis was performed using the revised ALE algorithm (Eickhoff et al. 2012; see Supplementary Methods I.3. for a description of the use of ALE for MACM). All resulting ALE scores were recorded. To take into account the complete brain-wide pattern of co-activation likelihood of each seed voxel, no height threshold was set at this point of analysis.

Connectivity-Based Parcellation Using Co-activation Patterns. The brain-wide co-activation profiles for all seed voxels were combined into a $N_S \times N_B$ connectivity matrix. N_S is the number of seed voxels (i.e., 4143 voxels) and N_B the number of target voxels in the reference brain volume at $4 \times 4 \times 4$ mm^3 resolution (26 459 gray matter voxels). Altogether, 37 individual connectivity matrices were computed, each representing the connectivity of the seed voxels for a given filter size.

K-MEANS CLUSTERING. In line with previous parcellation studies (Klein et al. 2007; Kelly et al. 2012; Clos et al. 2013), the parcellation was performed using *k*-means clustering (see Supplementary Methods I.4. for a description of *k*-means). In line with previous parcellation studies of multifunctional regions, we addressed a wide range of potential subdivisions (Kelly et al. 2010, 2012; Kahnt et al. 2012). That is, we searched for 2–11 different clustering solutions by making *k* ranging from 2 to 11, yielding 10 different clustering solutions within the right PMd (a 2-cluster solution, a 3-cluster solution, and so on, up to an 11-cluster solution). For each of the 370 (10 × 37) individual parcellations, the best solutions from 500 replications with a randomly placed initial centroid were computed. Q3

SELECTION OF THE OPTIMAL RANGE. Like in a previous study (Clos et al. 2013), the optimal filter range was chosen based on the consistency of each voxel's cluster assignment across the different filter sizes. Those analyses are reported in Supplementary Methods I.5. In all subsequent steps, the analysis was restricted to the parcellations based on co-activations as estimated from the nearest 85 to 145 experiments.

DATA-DRIVEN SELECTION OF THE OPTIMAL CLUSTERING SOLUTION. In the next step, we determined the optimal clustering solution, that is, the parcellation that was most supported by the data. This choice was based on 3 criteria: 1) variation of information, 2) percentage of deviants, and 3) silhouette value. The full description of these criteria is provided in Supplementary Methods I.6. The above criteria identified a 5k solution as the most stable parcellation of the right PMd.

Parcellation Based on Probabilistic Diffusion Tractography (PDT-CBP). *Data Acquisition and Preprocessing*. Diffusion weighted imaging (DWI) data of 20 healthy adults were acquired using a 3.0 T GE MR Scanner (see Wang et al. 2015 for a full description of the data sample and acquisition parameters). The data were preprocessed using FMRIB's Diffusion Toolbox (FSL 4.0; http://www.fmrib.ox.ac.uk/fsl). The T_1 images obtained in diffusion space were transformed to the ICBM-152 brain template while an inverse transformation was performed to transform the VOI masks of the right PMd into the diffusion space for each subject.

Diffusion probabilistic tractography was performed using the FSL package for each voxel in the PMd seed VOI to estimate the connectivity probability as described in Wang et al. (2015).

Cross-Correlation Matrix, Parcellation, and Maximum Probability Map of the k *Solution*. Cross-correlations (dimensions: number of seeds × number of seeds) between the connectivity patterns of all voxels in the PMd seed VOI were calculated. The cross-correlation matrix was then permutated using spectral clustering (not spectral reordering). An edge-weighted centroidal Voronoi tessellations method for automated clustering was applied to define 5 clusters as revealed as the most stable cluster solution for MACM-CBP. Then, the maximum probability maps were created for each *k* solution across all the subjects (see Wang et al. 2015 for a full description of the CBP pipeline).

Parcellation Based on RSFC (RSFC-CBP). *Data Acquisition and Preprocessing*. EPI resting state data from 124 healthy subjects (age range: 18–59, mean ± standard deviation: 39.5 ± 11.5, 66 males) were acquired as part of the 1000 brains study (Caspers et al. 2014). A description of acquisition parameters is provided in Supplementary Methods I.7. Functional image processing was performed using SPM8 (Wellcome Trust Centre for Neuroimaging, London, http://www.fil.ion.ucl.ac.uk/spm/software/spm8). Prior to further analyses, the first 4 scans were discarded. Then, preprocessing of the EPI images included affine registration and normalization to MNI space using unified segmentation approach. A more comprehensive description of this procedure is available in Supplementary Methods I.7.

Cross-Correlation Matrix, Parcellation, and Maximum Probability Map of the k Solution. The time series were computed for each voxels when removing potentially noisy variance (see Supplementary Methods I.7. for a description of the procedure). Linear (Pearson) correlations between the time series of each seed voxels (cluster) and all other gray matter voxels were computed and z-transform to quantify RSFC. The individual connectivity matrices of the seeds voxels with the whole-brain gray matter voxels. *k*-Means (with *k* ranging from 2 to 9) was then performed on the individual connectivity matrices. Finally, the maximum probability maps were created for each *k* solution across all the subjects.

Multimodal Functional Connectivity of the MACM-CBP-Derived Clusters

Following the parcellations of the seed region, we examined the functional connectivity profile of each cluster by performing additional MACM and RSFC analyses of the obtained clusters. While MACM provides the co-activation pattern of the clusters across a wide range of active tasks, RSFC provides the complementary, task-free measure of functional connectivity of these clusters (Eickhoff et al. 2011).

We first computed the whole-brain connectivity pattern of each cluster and then examined the commonalities among clusters as well as the differences between them. In other words, for each modality (MACM and RSFC), we statistically tested both the conjunction of all clusters and the contrasts between them.

Task-Related Functional Connectivity (MACM). *Main Effects*. For each obtained PMd subregion, an ALE meta-analysis was performed across all BrainMap experiments featuring at least one focus of activation within each of the derived clusters using the same approach as described above. In contrast to the MACM underlying CBP, where ALE maps were not thresholded to retain the complete pattern of co-activation likelihoods, we now performed statistical inference by testing the observed ALE scores from the actual meta-analysis against ALE scores obtained under the null distribution of random association of foci between experiments. A full description of this procedure is provided in Supplementary Methods I.8. This test yielded a *P* value based on the proportion of equal or higher random values. The resulting nonparametric *P* values were transformed into z-scores and thresholded at a cluster level with family-wise error rate (FWE)-corrected $P < 0.05$ (cluster-forming threshold at voxel level: $P < 0.001$).

To identify task-related co-activation common to all clusters, we computed the overlap between the brain-wide co-activation patterns of all MACM-CBP-derived clusters using a minimum-statistic conjunction (Nichols et al. 2005).

Contrasts. To compare the brain-wide co-activation pattern between clusters, we first computed the voxel-wise differences between the ensuing ALE maps. Each of these difference scores was then compared with a null distribution. A full description of this procedure is provided in Supplementary Methods I.8. This test yielded a posterior probability *P* testing that the difference was not due to random noise in an exchangeable set of labels based on the proportion of lower differences in the random exchange. The resulting probability values were then thresholded at $P > 0.95$ (95% chance for true difference) and masked by the respective main effects, that is, the significant effects of the MACM for the minuend (e.g., the difference "Cluster ~~1~~ – Cluster ~~2~~" was inclusively masked by the main effect of Cluster ~~1~~).

Finally, we computed the specific co-activation pattern for all derived clusters, that is, brain regions significantly more co-activated with a given cluster than with any of the other clusters. This was achieved by performing a minimum-statistic conjunction across the results of the 4 contrasts between a given cluster and the remaining others.

RSFC for Each Cluster

RSFC analyses were performed on the normalized resting-state fMRI images as described at 2.2.3.1. and in Supplementary Methods I.7. These latter were first smoothed by a 5-mm full-width at half-maximum (FWHM) Gaussian kernel to improve signal-to-noise ratio and to compensate for residual anatomical variations.

Time series of the seed region were extracted for all gray matter voxels. The cluster time course was then expressed as the first eigen variate of these voxels' time courses. Linear (Pearson) correlations between the time series of each seed region (cluster) and all other gray matter voxels were computed to quantify RSFC. These voxel-wise correlation coefficients were then transformed into Fisher's z-scores. These Fisher's z-scores were entered into a flexible factorial model to test for consistency across subjects, testing for the significance of the main effects of connectivity for each cluster as well as the differences between the clusters.

The CBP-derived clusters were used as seeds for the RSFC analyses. In correspondence with the MACM analyses described above and in line with previous studies (Clos et al. 2013), we first calculated RSFC shared by all MACM-CBP-derived clusters. This was achieved by computing a conjunction across the main effect of positive connectivity of all clusters. Second, we examined the specific co-activation pattern of each cluster. These patterns were obtained by performing a conjunction analysis, for each cluster, across the contrasts between the main effect of a given cluster and all other clusters. All analyses were thresholded at $P < 0.05$ (cluster FWE-corrected, cluster-forming threshold: $P < 0.001$).

Shared Task-Related and RSFC: Conjunction Across MACM and RSFC Results

For cross-validation, the results shared between both MACM and RSFC analyses were then examined for each cluster using a minimum-statistic conjunction. This procedure aimed to characterize the whole-brain connectivity pattern that is similar in resting state and in MACM (cf. Bzdok et al. 2013; Cieslik et al. 2013; Clos et al. 2013). We performed the conjunction between RSFC and MACM for 1) Common pattern for all clusters and 2) Specific pattern of each cluster (i.e., differences between clusters). For all these conjunction analyses, only cluster extend ≥10 voxels were further reported.

Functional Characterization of the MACM-CBP-Derived Clusters

Forward and Reverse Inference on BrainMap Meta-data

Functional characterization of the right PMd clusters revealed by MACM-CBP was performed using the "behavioral domain" (BD) and "paradigm class" (PC) meta-data of the included experiments as assigned in the BrainMap database (Laird et al. 2009). A description of the behavioral processes covered by the Brainmap paradigm class taxonomy may be found at http://brainmap.org/taxonomy/paradigms.html. BDs include the main categories "cognition, action, perception, emotion, interoception," as well as their respective subcategories. In turn, PCs categorize the

specific task employed. To characterize the individual functional profile of each cluster, we performed quantitative "forward inference" and "reverse inference" as has been done in previous parcellation studies (Bzdok et al. 2013; Cieslik et al. 2013; Clos et al. 2013). In the forward inference approach, a cluster's functional profile is assessed by identifying taxonomic labels for which the probability of finding activation in the respective cluster is significantly higher than finding activation for that label across the whole database by chance. Significance was determined using a binomial test ($P < 0.05$ corrected for multiple comparisons using Bonferroni's method; Clos et al. 2013; Rottschy et al. 2013). That is, we tested whether the conditional probability of activation in a particular region given a particular label [P(Activation|Task)] was higher than the baseline probability of activating this particular region [P(Activation)]. In the reverse inference approach, a cluster's functional profile was determined by identifying the most likely BDs and PCs given activation in a particular cluster, that is, the likelihood P(Task|Activation). This likelihood can be derived from P(Activation|Task) as well as P(Task) and P(Activation) using Bayes' rule. Significance (at $P < 0.05$, corrected for multiple comparisons) was then assessed by means of a χ^2 test. In sum, forward inference assessed the probability of activation given a behavioral label, whereas reverse inference assessed the probability of each behavioral label given an activation.

As done previously, we also performed contrast analyses between the different clusters' functional profiles. These contrasts were, in turn, constrained to those experiments in BrainMap activating either cluster. From this pool of experiments, the base rate is the a priori probability of any focus to lie in either of the 2 compared clusters given that it is located in any of them. Forward inference here compared the activation probabilities between the 2 clusters given a task compared with the a priori base rate. This was again achieved by means of a binomial test ($P < 0.05$, corrected for multiple comparisons). In the reverse inference approach, we compared the occurrence probabilities of the tasks given activation in 1 cluster (rather than in the other). This probability comparison was again achieved by means of a χ^2 test ($P < 0.05$, corrected for multiple comparisons).

Results

Cortical Parcellation Based on Connectivity Pattern

As our study aimed to distinguish functional subregions (i.e., clusters) in the right PMd, we first examined the most stable cluster solution obtained with CBP based on MACM across a wide range of k-solutions (from $k = 2$ to $k = 11$). We then investigated whether the topographical organization revealed by the ensuing solution could be supported by CBP based on other modalities. In particular, we performed PDT-CBP and RSFC-CBP, again evaluating different cluster solutions (in the vicinity of the $k = 5$ solution found for MACM) based on their inter-subject stability.

Cortical Parcellation Based on Co-activation Pattern (MACM-CBP)

The information, separation, and consistency criteria jointly identified the 5-cluster (5k) solution as the best among the 10 k-means clustering solutions. The splitting of the 5 clusters into functional space is illustrated in Supplementary Figure 3 and described in Supplementary Results II.1 while the resulting 5 clusters are illustrated in Figure 2A.

The rendering of the 5 clusters separately on coronal plans with the respective number of voxels and MNI coordinates of their respective center of gravity are illustrated in Supplementary Figure 3B. In addition, MNI coordinates of their borders are listed in Supplementary Results II.2, and the derived subregions in MNI volume space are available at http://anima.fz-juelich.de/studies/Genon_CBPrightPMd_2016. The location of the clusters highlights a rostro-caudal organization along the superior and middle frontal gyri. This organization includes a rostral cluster that lies anteriorly to the precentral gyrus; a central cluster that lies at the intersection of the precentral sulcus and the superior/middle frontal gyri; and a caudal cluster that is located at the posterior

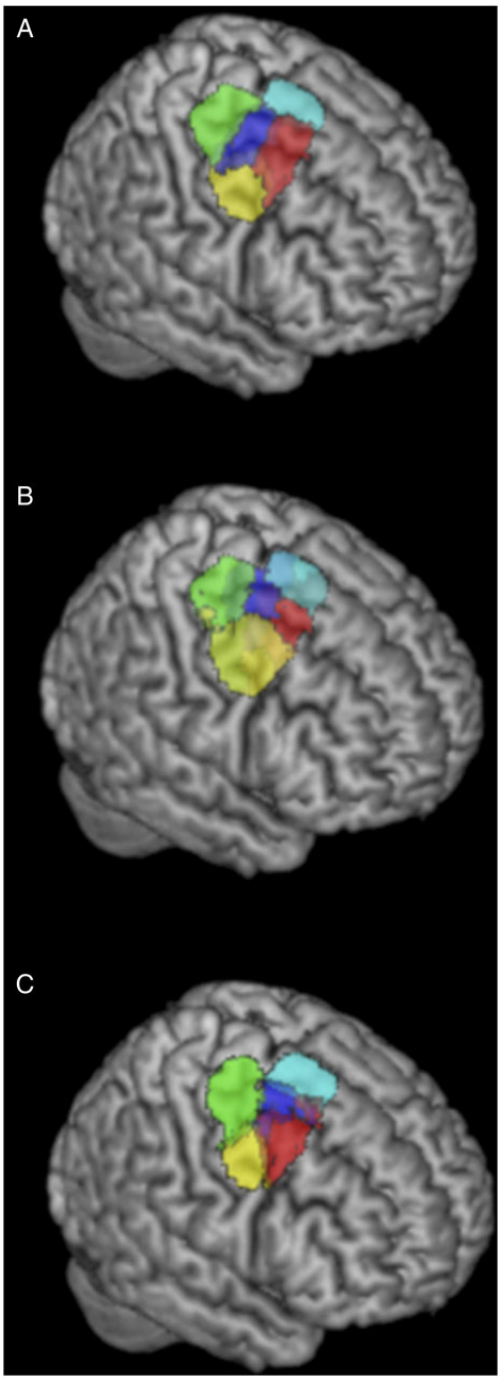

Figure 2. Rendering of the 5k solution yielded by different CBP modalities in the right PMd. (*A*) 5k solution yielded by MACM-CBP. (*B*) 5k solution yielded by PDT-CBP. (*C*) 5k solution yielded by RSFC-CBP.

part of the precentral gyrus. The location of the clusters further suggests a ventrodorsal organization with a ventral cluster adjacent to ventral PM and mainly overlapping with the precentral gyrus; the previously mentioned central cluster; and a dorsal cluster adjacent to inter-hemispheric premotor areas. For convenience, hereafter the clusters are labeled according to their anatomical location (i.e., rostral, caudal, central, ventral, and dorsal).

5-Cluster (5k) Solution Revealed by Structural Connectivity Pattern (PDT-CBP) and Unconstrained Functional Connectivity (RSFC-CBP)

The 5k solution identified by PDT-CBP showed good correspondence with the 5k solution identified by MACM-CBP with both rostro-caudal and ventrodorsal differentiation and a centrally located cluster (Fig. 2*B*). ~~Based on the topographical similarities between the 5 MACM-CBP derived cluster and the 5 PDT-CBP clusters, we computed the percentage of overlap between each pair of corresponding cluster. Those results are available in Supplementary Table 1.~~

The 5k solution yielded by RSFC-CBP is illustrated in Figure 2*C*. Matching MACM-CBP and PDT-CBP, it revealed a rostro-caudal organization and a ventrodorsal organization including and a centrally located cluster on the superior posterior frontal sulcus. We nevertheless note that the rostral and central border are less differentiated at the location of the superior frontal sulcus emphasizing that the rostro-caudal organization should be considered in term of gradient and not as spatially segregated subregions.

Examination of the stability of PDT-CBP-derived parcellation across resampling (half split) revealed that several k solutions show good stability. In particular, stability significantly increases (as reflected by both Cramer V and Normalized Mutual Information) from $k = 3$ to $k = 4$ and from this latter k solution to $k = 5$. In contrast, stability does not increase from $k = 5$ to $k = 6$ suggesting that we reach a local optimum at $k = 5$. Thus, the 5k solution is relatively well supported by DWI data. In contrast, examination of percentage of deviants and silhouette value across subjects indicated a general pattern of slightly linearly decrease of stability/consistency as k increases in RSFC-CBP. Nevertheless, examination of VI between subjects across k solutions showed that while VI tends to decrease from $k = 4$ to $k = 5$, it significantly increase from $k = 5$ to $k = 6$ suggesting that we also reach a local optimum at $k = 5$ with RSFC-CBP.

The overlap in term of number of voxels in the voxels between the 5k parcellation revealed by MACM-CBP and the 5k parcellation revealed by the 2 other CBP modalities is described in Supplementary Results III.3.

Functional Connectivity of the Clusters Yielded by MACM-CBP

Common Functional Connectivity Patterns

The functional connectivity profile common to all clusters across both MACM and RSFC as well as functional connectivity profile common to all clusters only revealed by MACM are detailed in Table 1.

The results of the conjunction across the functional connectivity patterns of all 5 clusters across both MACM and RSFC analyses identified 2 regions common to all 5 clusters: postero-medial frontal cortex (SMA/pre-SMA) and the central cluster. That is, aside from common local connectivity with the central cluster, the postero-medial frontal cortex was the only brain region that showed consistent functional coupling with all identified clusters. Nevertheless, examination of the connectivity profile only observed by MACM additionally revealed that all clusters were co-activated with the bilateral IPS [Area hIP2/hIP3 (Choi et al. 2006)], the bilateral Area 44 (Amunts et al. 1999), the bilateral anterior insula, the bilateral prefrontal thalamus (Behrens et al. 2003), and the right pallidum. In contrast, RSFC revealed that all clusters were commonly coupled with the right rostral and ventral clusters and the primary somatosensory cortex [Area 2; (Grefkes et al. 2001)] extending to supramarginal gyrus [Area PFt (Casper et al. 2006, 2008)].

Cluster-Specific Functional Connectivity Patterns

Contrasting each cluster's functional connectivity patterns with those of all 4 other clusters identified each cluster's specific functional connectivity pattern. These findings are detailed in Table 1 and illustrated in Figure 3. For the sake of robustness of the highlighted functional connectivity profile, we mainly relied on the conjunction of unconstrained specific functional connectivity (as assessed with RSFC) and task functional connectivity (as assessed with MACM) as illustrated in Figure 3*C*. However, for the sake of completeness, we additionally examined the pattern yielded by ~~RSFC~~ (Fig. 3*A*) and the pattern yielded by ~~MACM~~ (Fig. 3*B*) separately. Nevertheless, the divergence between both approaches is discussed in Supplementary Discussion III.1.1.

Both approaches (RSFC and MACM) indicated specific connectivity of each cluster with a homotopic cluster in the left hemisphere. Each cluster showed additional specific connectivity profile reposted below.

Rostral Cluster. Both approaches showed that the rostral cluster was specifically connected to bilateral intraparietal sulcus [IPS: areas hIP1/hIP2 (Scheperjans et al. 2008)], lateral prefrontal cortex LPFC, midcingulate cortex and the right precuneus.

MACM further revealed that the rostral cluster was functionally coupled with the left ventral LPFC and the dorsomedial prefrontal cortex (DMPFC) while RSFC additionally revealed that it was functionally connected to the bilateral cerebellum lobule VII (Diedrichsen et al. 2009), the bilateral inferior temporal gyrus, the left precuneus, the right subiculum, and the right fusiform gyrus.

Caudal Cluster. Both approaches revealed that the caudal cluster was specifically connected to bilateral M1 [area 4p (Geyer et al. 1996)], bilateral SMA extending into midcingulate cortex, left cerebellum [lobule IV/V (Diedrichsen et al. 2009)], and right parietal operculum [areas OP1/OP3 (Eickhoff et al. 2006)] and frontal operculum.

MACM further revealed that the caudal cluster was functionally coupled with the posterior insula, the thalamus [premotor and prefrontal (Behrens et al 2003)], and the right putamen while RSFC additionally revealed functional connectivity of this cluster with parietal operculum subarea OP3/OP4 (Eickhoff et al. 2006).

Central Cluster. Both approaches showed that the central cluster was specifically connected to bilateral IPS (area hIP3) extending to superior parietal lobule [SPL: areas 7A/7PC/5l (Scheperjans et al. 2008)].

MACM further revealed that the central cluster was functionally coupled to the right fusiform gyrus [Area FG1/FG2 (Caspers et al. 2013)] and the left primary sensorimotor areas [Area 2 (Grefkes et al. 2001); Area 3b (Geyer et al. 1999)] while RSFC additionally revealed that it was functionally connected to left Broca's area [Area 44 (Amunts et al. 1999)], bilateral inferior parietal lobule [Area 2 (Grefkes et al. 2001); Area PFt & Area PFop; (Caspers et al. 2006, 2008)], and middle occipital gyrus.

Table 1 Common and specific functional connectivity of the 5 MACM-CBP-derived clusters across tasks (MACM) and rest (RSFC)

Region		Overlap with cytoarchitectonic area	x	y	z	Cluster size
Common to all clusters						
Tasks and rest						
Central cluster	R	NA	32	−3	57	107
Left PMd (central cluster's homotope)	L	NA	−33	−8	55	50
SMA/pre-SMA	L	NA	−8	5	51	58
	R	NA	5	8	49	13
	R	NA	6	4	64	10
Tasks only						
IPS	L	hIP3[i]	−34	−50	51	663
	R	hIP2/hIP3[d,i]	39	−47	50	189
Broca's area	R	Area 44[a]	54	9	28	305
	L	Area 44[a]	−53	6	31	256
Thalamus	R	Prefrontal thalamus[j]	12	−14	7	191
	L	Prefrontal thalamus[j]	−11	−16	7	171
Anterior insula	R	NA	36	23	1	165
	L	NA	−34	23	1	162
Basal ganglia	R	Pallidum/putamen	19	3	3	23
Rest only						
Rostral and ventral clusters	R	NA	26	−3	55	1369
Right somatosensory-cortex/supramarginal gyrus	R	Area 2[c]/Area PFt[l]	50	−32	48	301
Specific to rostral PMd						
Tasks and rest						
Left homotope	L	NA	−27	9	52	332
Middle frontal	L	NA	−40	29	33	166
Middle frontal	R	NA	30	8	42	1272[n]
			33	21	42	
			44	48	20	
			48	36	24	
		Fp1[b]	30	58	10	
MCC	R	NA	7	26	42	19
Inferior parietal/IPS	R	hIP1/hIP2[d]	42	−57	41	498
	L		−38	−58	41	389
Precuneus	R	NA	8	−62	50	63
Tasks only						
Inferior frontal gyrus	L	NA	−38	14	37	1071
	R	NA	32	29	−7	134
Rest only						
Inferior temporal gyrus	R	NA	62	−34	−18	601
	L		−57	−54	−15	160
Precuneus	L	NA	−6	−58	45	629
Cerebellum	L	Lobule VIIa[g]	−38	−65	−37	519
	R		34	−62	−33	100
Medial temporal lobe	R	Subiculum	29	−32	−18	318
Fusiform gyrus	R	NA	−30	−40	−14	193
Specific to caudal PMd						
Tasks and rest						
Primary motor	R	Area 4p[e]	34	−26	60	1492°
Cortex	L	Area 4p[e]	−36	−29	60	535°
Left homotope						
SMA/Midcingulate cortex	R	NA	8	−10	50	153
	L		−5	−16	53	67
Cerebellum	L	Lobule VI/V[g]	−18	−57	−20	350
Parietal operculum	R	Area OP1/OP3[h]	47	−21	20	78
Frontal operculum	R	NA	44	−3	14	16
Tasks only						
Putamen	R	NA	31	−6	−1	66
Thalamus	R	Prefrontal/premotor thalamus [j]	14	−19	8	60
Posterior insula	R	NA	43	1	12	44
Rest only						
Parietal operculum	L	Area OP3/OP4[h]	−42	−21	18	366

Continued

Table 1 Continued

Region		Overlap with cytoarchitectonic area	x	y	z	Cluster size
Specific to central PMd						
Tasks and rest						
IPS/superior	R	Area 7A[i]/Area7PC[i]/hIP3[i]	26	−58	57	405
Parietal lobule	L	Area 7A[i]/Area 7PC[i]/Area 5l[i]	−28	−56	61	335
		Area 7A[i]	−19	−75	44	71
			−14	−67	58	33
Left homotope	L	NA	−25	−8	56	553
Tasks only						
Fusiform gyrus	R	Area FG1/FG2[k]	38	−68	−12	65
Somatosensori area	L	Area2[c]/Area 3b[e,f]	−38	−36	48	13
Rest only						
Inferior parietal lobule	R	Area2[c]/Area PFt[l]/Area PFop[l]	35	−41	48	1656
	L		−34	−44	47	1848
Middle occipital gyrus	L	NA	−23	−76	32	136
	R		29	−74	34	112
Broca area	L	Area 44[a]	−52	6	29	133
Specific to ventral PMd						
Tasks and rest						
Superior temporal	R	NA	59	−41	12	49
Left homotope	L	NA	−46	−4	48	356
Tasks only						
Visual cortex	R	hOc5[m]	50	−66	5	68
Rest only						
Inferior frontal	R	Area 45[a]	46	17	23	1277
Gyrus	L		−44	17	25	355
	R	NA	43	34	−7	259
Posterior middle	R	NA	60	−44	8	660
Temporal gyrus	L	NA	−58	−51	10	355
Specific to dorsal PMd						
Tasks and rest						
Left homotope	L	NA	−8	4	64	126
Inferior frontal gyrus/insula	R	NA	49	10	3	105
	L		−49	7	2	85
Putamen	R	NA	25	11	2	55
MCC	R	NA	10	10	40	22
Tasks only						
Broca's area	L	Area 44[a]	−52	10	3	505
	R	Area 44/45[a]	55	15	6	325
Rest only						
Middle frontal gyrus	R	NA	27	48	24	511
	L		−30	46	22	468
Anterior cingulate cortex	L	NA	−8	18	31	496
	R		9	20	30	462
Cerebellum	L	Lobule VIIa[g]	−42	−54	−33	139
Pre-SMA	R	NA	9	24	60	59

Note: NA, not assigned to any known probability map/not applicable.
[a]Amunts et al. (1999).
[b]Bludau et al. (in press).
[c]Grefkes et al. (2001).
[d]Choi et al. (2006).
[e]Geyer et al. (1996).
[f]Geyer et al. (1999).
[g]Diedrichsen et al. (2009).
[h]Eickhoff et al. (2006).
[i]Scheperjans et al. (2008).
[j]Behrens et al. (2003).
[k]Caspers et al. (2013).
[l]Caspers et al. (2006); Caspers et al. (2008).
[m]Malikovic et al. (2007).
[n]The region is part of the local connectivity of the rostral PMd itself (1083 voxels).
[o]The region is part of the local connectivity of the caudal PMd itself (1765 voxels) in the right hemisphere or its left-side homotope in the left hemisphere; CBP, Co-activation-based parcellation; MACM, meta-analytic connectivity modeling; RSFC, resting state functional connectivity; PMd, dorsal Premotor Cortex; IPS, intraparietal sulcus; SMA, supplementary motor area.

Ventral Cluster. Both approaches indicated that the ventral cluster was specifically connected to the right posterior superior temporal gyrus.

MACM further revealed that the ventral cluster was coactivated with right visual extrastriate cortex [hOC5 (Malikovic et al. 2007)] while RSFC showed that it was also connected to the bilateral posterior middle temporal gyrus and the bilateral ventral PFC [inferior frontal gyrus including Area 45 (Amunts et al. 1999)].

Dorsal Cluster. Both approaches indicated that the dorsal cluster was specifically connected to bilateral inferior frontal gyrus

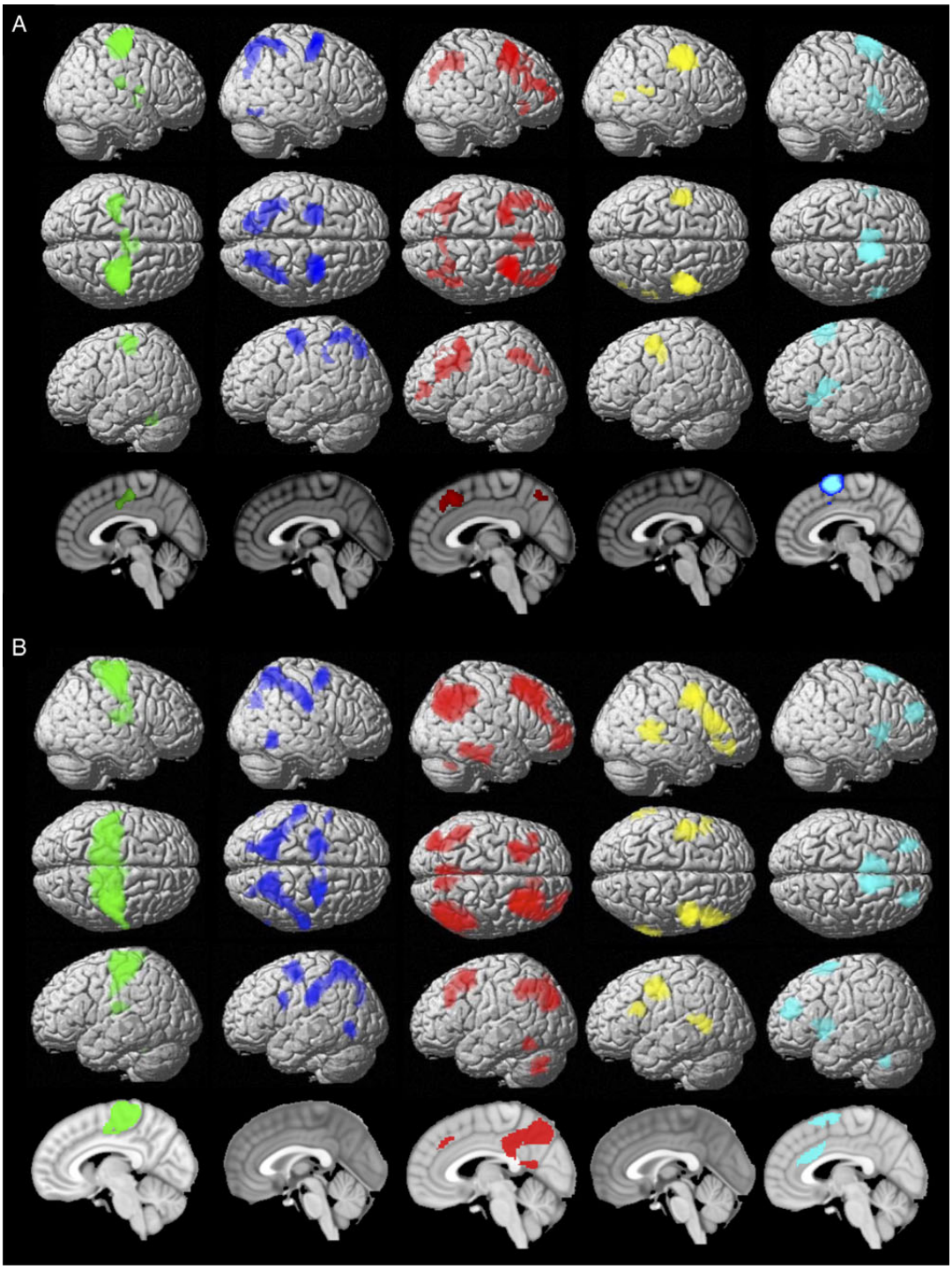

Figure 3. Specific functional connectivity profile of the MACM-CBP-derived subregions. Color code: green = caudal cluster, blue = central cluster, red = rostral cluster, yellow = ventral cluster, light blue = dorsal cluster. (*A*) ~~RSFC~~. (*B*) ~~Task functional connectivity (MACM)~~. (*C*) Conjunction of RSFC and MACM functional connectivity profile for each cluster.

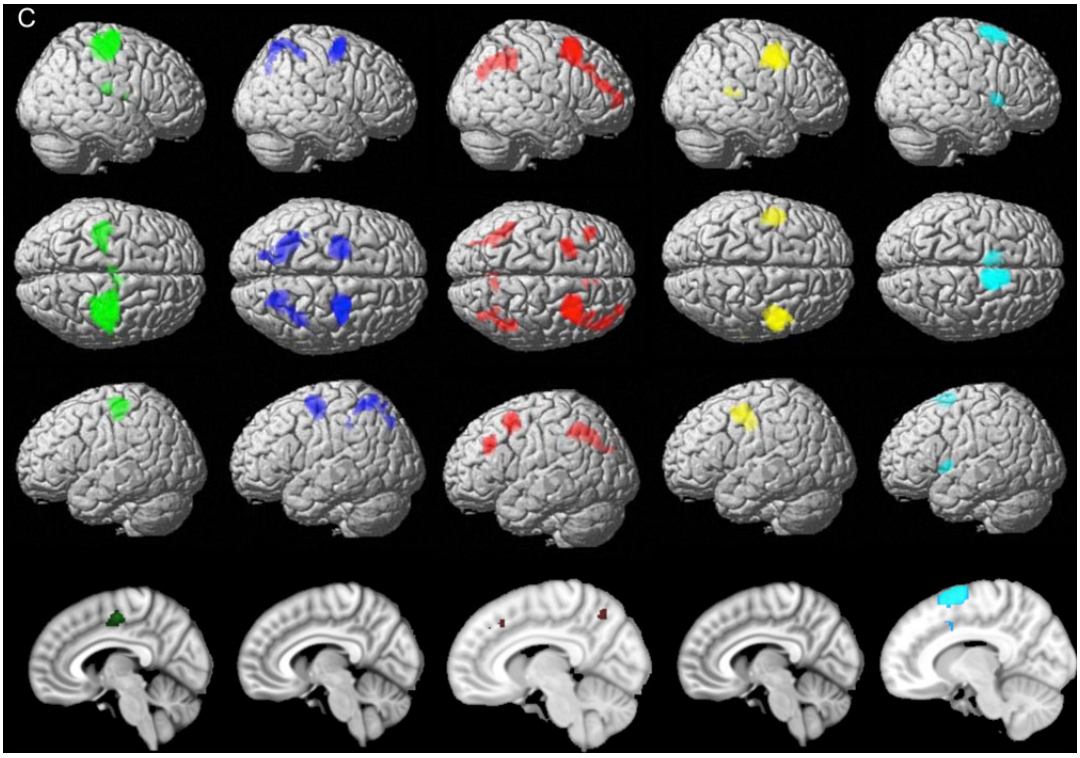

Figure 3. Continued.

slightly extending to the insula, the right putamen, and the right MCC.

MACM further revealed that the ventral cluster was coactivated with Broca's area [Area 44 (Amunts et al. 1999)] while RSFC revealed that it was functionally connected to middle frontal gyrus, bilateral ACC, left cerebellum [lobule VII, (Diedrichsen et al. 2009)], and right pre-SMA.

Functional Characterization of the Clusters Yielded by MACM-CBP

Forward and Reverse Inference on BrainMap Taxonomic Meta-data

Functional characterization of the 5 right PMd clusters was performed by forward and reverse inference on the taxonomic labels (BDs and PCs) provided by the BrainMap database (Laird et al. 2009). BDs and PCs significantly associated with each cluster across both forward and reverse inference are illustrated in Figure 5 and summarized in Figure 4. A description of the behavioral processes covered by the Brainmap paradigm class taxonomy may be found at http://brainmap.org/taxonomy/paradigms.html.

As shown in Figure 4A, some paradigms appeared to be related to several clusters across both forward and reverse inference. In particular, the central cluster showed a common paradigm profile with the caudal cluster regarding the PCs finger tapping and drawing. In addition, it showed a common paradigm profile with the rostral and ventral clusters regarding saccades and anti-saccades. Furthermore, the central and rostral clusters showed a common association with the PC "mental rotation." Finally, it shared visual distractor processing/visual attention with the ventral cluster.

Furthermore, there were several PCs specifically related to ~~a~~ particular cluster. In particular, cognitive paradigms such as the *n*-back task or the Wisconsin Card Sorting Test were specifically related to the rostral cluster. In contrast, paradigms targeting basic motor performance, such as finger flexion/extension or isometric force paradigms, were specifically related to the caudal cluster. Finally, imagined movements, sequence learning, and visual pursuit/tracking paradigms were specifically associated with the central cluster.

Synthesizing these findings, the functional characterization according to PCs thus revealed that the rostral cluster was mainly associated with paradigms engaging higher cognitive functions such as working memory. In contrast, the caudal cluster was mainly related to paradigms targeting motor functions. In turn, the ventral cluster was mainly associated with visual attention and eye movement paradigms, whereas the dorsal cluster was preferentially associated with paradigms engaging hand movements such as finger tapping. Finally, the central cluster showed a mixed pattern of associations including paradigms targeting motor functions, visual attention/eyes movements, and spatial cognition.

As illustrated in Figure 4B, the functional characterization according to BDs of the BrainMap database corroborated the above-described pattern emerging from the PC analysis and furthermore showed that while the central cluster was specifically associated with action imagination, the ventral cluster was specifically associated with vision.

The likelihood ratio and probabilities values associated to each significant behavioral label for each cluster are illustrated in Figure 5 while the results of the contrast analyses between the different clusters' functional profiles are illustrated in Figure S4. These results revealed a cognitive-motor gradient along the rostro-caudal axis. The rostral cluster was more related to higher cognitive functions than the central one, which was, in turn, more related to higher cognitive functions than the caudal one. For example, the rostral cluster was more related to working memory than the central one, but this latter was more associated

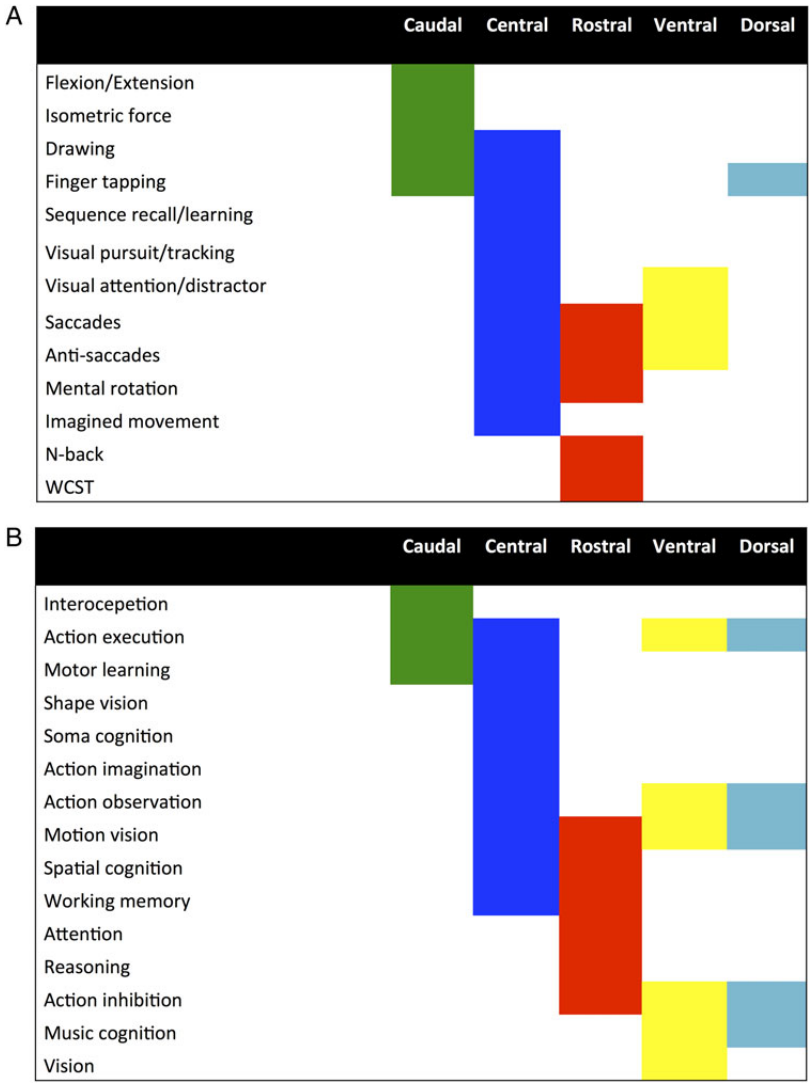

Figure 4. Summary of functional characterization of the clusters yielded by MACM-CBP as jointly reflected by forward and reverse inference. (*A*) Functional characterization according to the BrainMap paradigm classes. (*B*) Functional characterization according to the BrainMap behavioral domains.

with working memory than the caudal cluster. Motor functions showed the opposite pattern. For example, the caudal cluster was more associated with action execution than the central one, but this latter was more associated with action execution than the rostral cluster.

The contrast analyses furthermore highlighted that the ventral cluster showed the strongest association with eye movements/visual attention. Interestingly, the contrast analyses also showed that both the ventral and dorsal clusters were more related to speech functions than the rostral and the central ones. In addition, the dorsal cluster was more related to music cognition than the rostral and caudal clusters. However, the ventral and dorsal clusters differed in their functional profiles since the contrast between them revealed that while the ventral one was more associated with eye movements/visual attention, the dorsal one was more related to finger tapping.

Discussion

Using MACM-CBP, we found 5 distinct clusters within right PMd, which were corroborated by complementary structural and resting-state functional clustering approaches. Furthermore, by combining task-related (MACM) and task-free (RSFC) analyses, we characterized the whole-brain functional connectivity patterns of these 5 clusters. We finally used a meta-analytic approach to assign each of the 5 clusters a specific behavioral functional profile that complements the observed parcellation.

Consistent PMd Clustering Patterns Across Modalities

After testing a range of possible granularities based on co-activation patterns across studies (MACM), the 5-cluster (5k) solution was found to be optimally stable. It is noteworthy, however, that the choice of the cluster solution is an ill-posed problem (Eickhoff et al. 2015; Ryali et al. 2015), particularly since brain activity is likely characterized by multiple levels of organization (Bellec ~~2013~~). While we focused here on ~~1~~ particular scale, consideration of other scales may well provide additional insight into the neurobiological organization of the right PMd.

The selected 5k solution consisted of 1) a rostral cluster adjacent to prefrontal cortex, 2) a central cluster at an intermediate location (and adjacent to all other ones), 3) a caudal cluster adjacent

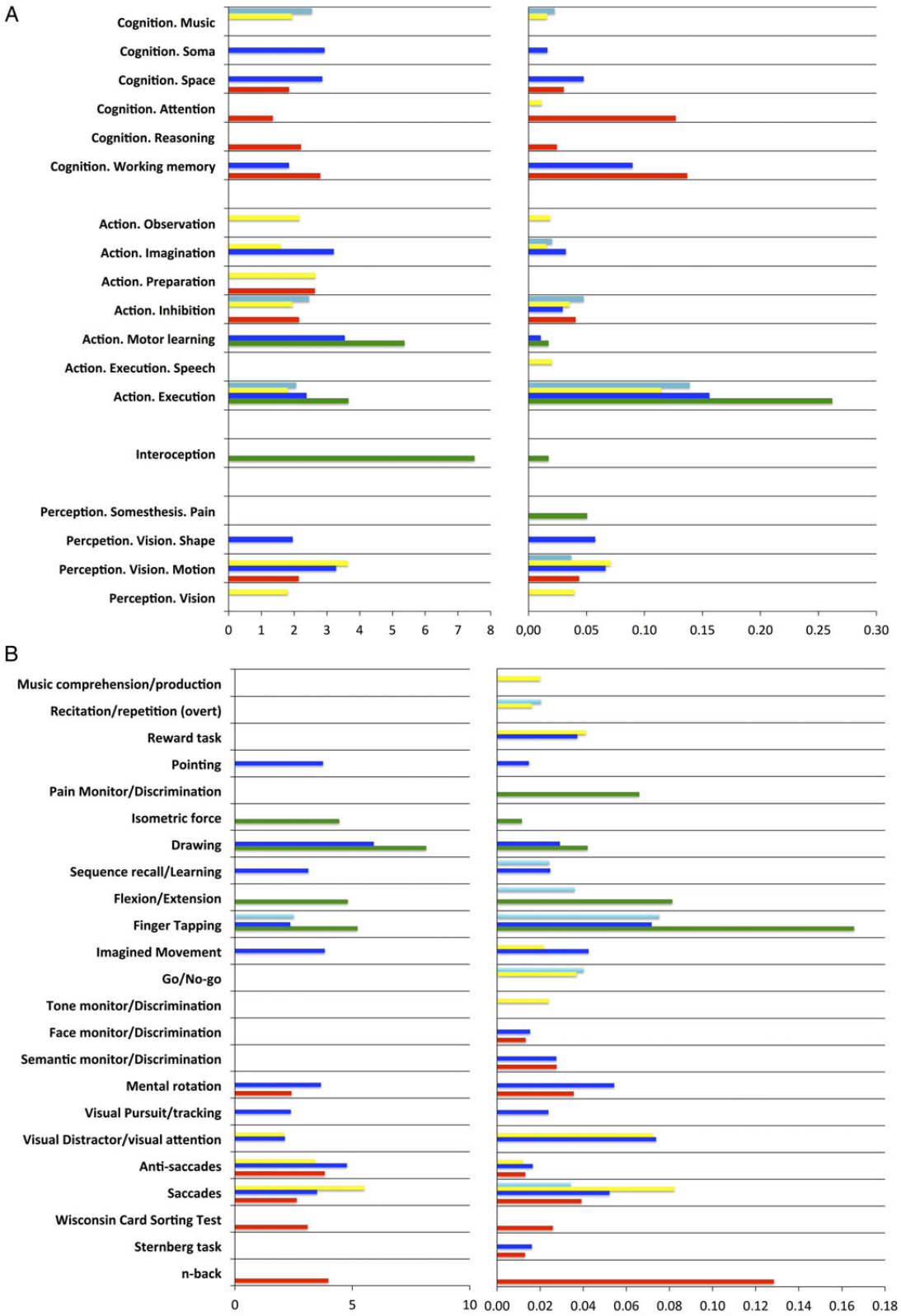

Figure 5. Functional decoding of the 5 right PMd clusters according to Brainmap. Functional decoding following forward inference expressed as likelihood ratio (left) and reverse inference expressed as probabilities (right). Color code: red, rostral; blue, central; green, caudal; yellow, ventral; light blue, dorsal. (A) Behavioral domains. (B) Paradigm classes.

to M1, 4) a ventral cluster adjacent to the PMv, and 5) a dorsal cluster bordering the medial premotor areas. This organization of the right PMd along both rostro-caudal and ventrodorsal axes was corroborated by additional parcellations based on structural connectivity (PDT) and unconstrained functional connectivity (RSFC). This cross-modal convergence suggests that the spatial organization of the right PMd revealed by MACM-CBP is robust across structural and functional criteria. It is important to highlight that the clusters' respective borders did not perfectly match across CBP modalities, suggesting that our methods have identified a topographical organization rather than a rigid set of borders. In particular, the rostro-caudal organization may be reflective of a gradient rather than sharply segregated subregions. Such a gradient mirrors the rostro-caudal organization suggested in nonhuman primates (see below) and corroborates at least one previous fMRI study in humans, in which it was associated with a cognitive-motor gradient (Orban et al. 2014).

Five Functional Subregions Within the Right PMd

Rostral PMd: Higher Cognitive Processes

Both the MACM and RSFC analyses revealed that the rostral PMd cluster was specifically functionally coupled with the midcingulate cortex, bilateral LPFC, and the IPS/inferior parietal regions. These regions are known to support higher cognitive functions such as executive functions (Collette et al. 2006), vigilant attention (Langner and Eickhoff 2013), and working memory (Rottschy et al. 2012). This cluster was also functionally connected with the precuneus, a region that is known to play a role in higher order visuospatial processes such as covert shift of attention and abstract mental imagery tasks (Cavanna and Trimble 2006). In line with this view, functional characterization across forward and reverse inference revealed that this cluster was engaged in functions such as working memory. In other words, the rostral cluster might be engaged in higher, potentially dynamic aspects of visuospatial imagery, which may possibly include short-term memory encoding of a location (Langner et al. 2014), maintenance of spatial information (including spatial rehearsal), and spatial updating. This cluster might also play a role in working memory even when the content is not overtly spatial (Nee et al. 2013).

The rostral cluster reported here bears similarity to area F7, the rostral subdivision of the PMd in nonhuman primates (Matelli et al. 1985, 1991). This region predominantly receives prefrontal inputs (Boussaoud et al. 1995; Rizzolatti and Luppino 2001) and contains neurons that are active when the animal engages cognitive functions such as spatial attention or memory (Boussaoud 2001; Lebedev and Wise 2001). In humans, a similar rostral PMd subregion, termed "pre-PMd," has been proposed, and connectivity between the pre-PMd and the prefrontal cortex has been suggested (Picard and Strick 2001). Similarly, previous functional studies have demonstrated that the most rostral part of the PMd (or pre-PMd) is frequently engaged in high-level cognitive operations (Hanakawa 2011), such as complex mental calculations (Zago et al. 2001). This evidence implies that our rostral cluster roughly corresponds to the proposed human pre-PMd and may be considered a potential homologue to F7 in the nonhuman primate. Of note, as there is currently no widely accepted landmark separating PM and prefrontal cortex, the rostral cluster found in the present study cannot be strictly considered a premotor region. In our study, the location of the rostral cluster, which is anterior to the precentral gyrus, leads us to consider it a transitional region in the ill-defined premotor-prefrontal dichotomy. Furthermore, its behavioral functional profile supports its consideration as a functional component of the prefrontal cortex, rather than a premotor module sensu-stricto.

Caudal PMd: Motor Functions

Task-based and RSFC analyses revealed that the most caudal PMd cluster is likely part of the brain's motor system, including bilateral M1, SMA, and the left cerebellum. The caudal cluster was also specifically functionally connected to right fronto-parietal operculum, which has been shown to support higher order somatosensory and sensorimotor processing (Eickhoff et al. 2010). Supporting this view, functional characterization of the caudal cluster revealed that it is engaged in action execution, motor learning, and interoception. It is thus likely that several functions that have frequently been assigned to the whole PMd are primarily subserved by this caudal subdivision. Such processes include 1) the creation of internal representations of action (or pragmatic body maps) which serve movement generation, understanding, and learning (Rizzolatti and Luppino 2001; Schubotz and von Cramon 2003), and 2) the organization of movement or action formulation (Schubotz and von Cramon 2003).

In line with our finding of a caudal cluster adjacent to M1 in humans, the posterior PMd adjacent to M1 in nonhuman primates has been defined as a distinct cytoarchitectonic and functional area. This caudal subregion, termed F2, is connected to M1 and the spinal cord (for reviews, see Geyer et al. 2000; Abe and Hanakawa 2009). The caudal PMd subregion has shown a similar connectivity pattern in humans, and fMRI studies have suggested that this subdivision (also referred to as the "PMd proper") is preferentially activated during movement preparation and execution (for a review, see Picard and Strick 2001). Such findings suggest a functional profile for the human caudal PMd which is similar to the one observed in nonhuman primates (Boussaoud 2001) and consistent with the one identified here for our caudal PMd cluster. Therefore, according to its integration into the sensorimotor network and its functional profile, characterized by processes related to motor preparation and programming, the caudal cluster may correspond to the nonhuman primate's caudal right PMd (area F2) and human right PMd proper.

Central PMd: the Core PMd

The central cluster was located between the rostral and caudal ones. Compared with all other clusters, it consistently showed a stronger functional coupling with the IPS and the SPL, regions that are known to be engaged in top-down/goal-driven modulatory processes (Corbetta and Shulman 2002). Considered separately, the MACM analysis further yielded connectivity with 2 different subregions of the ventral visual stream [respectively, FG2 and FDG1 (Caspers et al. 2015)]. Functional decoding revealed that the central cluster was related to both motor and cognitive functions (such as action execution and working memory), as well as to spatial cognition and motion perception. Together, these findings and the observation that all other clusters were functionally coupled with the central cluster suggest that the latter plays a core role within the right PMd mosaic by linking the functionally more specialized clusters within the right PMd.

Studies in nonhuman primates have also suggested a transitional region that lies at the border between F7 (i.e., rostral PMd) and F2 (i.e., caudal PMd), which has been named F2vr (for a review, see Abe and Hanakawa 2009). F2vr receives inputs from dorsolateral prefrontal cortex (DLPFC) and medial IPS (Luppino et al. 2003) and has been assumed to support the integration of a visuospatial parameter (target object) and a somatosensory/motor parameter (arm) to complete a motor plan (for a review,

see Abe and Hanakawa 2009). F2vr may thus subserve sensorimotor transformations. Our study provides support for the existence of a similar transitional cluster in humans within a central location, lying between the rostral "cognitive" cluster and the caudal "motor" one. Functional decoding showed that this subregion in human PMd is engaged in target and goal maintenance (working memory), visuospatial processes, action imagination, and action execution. This pattern suggests that our central cluster may, partly, include the human homologue of F2vr.

Ventral PMd: Eye-Related Functions

According to the functional decoding, the ventral and central PMd clusters shared several features. In particular, both were associated with saccades, anti-saccades, and visual attention paradigms. However, only the ventral cluster was significantly associated with the broader behavioral domain of vision. This behavioral profile fits with the specific co-activation of this latter cluster with the right visual cortex (see Supplementary Discussion III.2.1. for further discussion of task and rest functional connectivity of this cluster). These findings argue in favor of the ventral cluster being preferentially related to "eye-centered" functions. Such functions may cover learning sequences of eye movements, serial visual search, and visual attention. Nevertheless, the ventral cluster also showed broader associations, such as with action execution and action inhibition. Thus, while our ventral cluster may not strictly be considered an "eye field," it does likely overlap with the "premotor eye field" (see Supplementary Discussion III.2.2 for a description of the premotor eye field).

Dorsal PMd: Hand Preferences and Sequencing/Rhythm Aspects

In our MACM-CBP analysis, the dorsal PMd cluster was found to be closely coupled with the ventral cluster (see Supplementary Results II.1 and Supplementary Discussion III.1.2.). However, both PDT-CBP and RSFC-CBP clearly differentiated this dorsal subdivision as a separate cluster. Both MACM and RSFC identified specific functionally connectivity of this subdivision with bilateral prefrontal regions, insula, right putamen, and right MCC. These findings indicate that the dorsal cluster may be engaged in both motor and cognitive networks. Congruently, functional decoding showed a profile of associations that included motor, language, and music domains. Within the domain of motor functions, the dorsal cluster seemed to be preferentially related to hand/finger movements (i.e., finger tapping paradigms). In line with these findings, this part of the PMd was found to be activated for imitation of hand movements in a previous meta-analysis (Caspers et al. 2010). Our findings thus suggest that the dorsal cluster is related to both cognitive and motor processes, but appears to be particularly related to hand/finger movements, music, and language processing. There is evidence that music processing, language processing, and tapping might be related in certain respects (Overy et al. 2003); in particular, they may share sequencing and rhythm-processing aspects (Petkov et al. 2005; Flaugnacco et al. 2014). Therefore, although future studies are needed to more finely specify the motor and cognitive processes selectively engaging the dorsal cluster; for the time being, one can assume that this dorsal subregion preferentially supports sequencing and rhythm-processing aspects common to finger movements, music, and language.

Conclusion

Previous studies have suggested that the right PMd supports a wide range of motor and cognitive functions that may be topographically organized within this region, characterized by spatial gradients. Based on a quantitative data-driven approach, we showed that the right PMd can be robustly subdivided into 5 distinct functional modules. Our work highlighted a rostro-caudal organization with a rostral subregion supporting higher cognitive functions, a caudal subregion relatively more associated with motor functions, and a central subregion that may act as an interface between the rostral-cognitive and the caudal-motor subregions. Our study further revealed a ventrodorsal organization, including a ventral subregion that supports eye-field functions, a dorsal subregion that is preferentially related to hand/finger movements, and rhythm/sequencing aspects in cognitive and motor functions. How those modules may dynamically interact is discussed in Supplementary Discussion III.2.4. Finally, we suggest that the central subregion, positioned at the cross-roads of both gradients, plays an integrative role within this right PMd functional mosaic.

Supplementary Material

Supplementary material can be found at: http://www.cercor.oxfordjournals.org/.

Funding

The research leading to these results has received funding from the European Union Seventh Framework Programme (FP7/2007-2013) under grant agreement no. 604102 (Human Brain Project), the Deutsche Forschungsgemeinschaft (DFG, EI 816/4-1, EI 816/6-1, LA 3071/3-1), and the National Institute of Mental Health (R01-MH074457).

Notes

Furthermore, we thank Dr Matthew Glasser, Dr Saad Jbabdi, Dr Ricarda Schubotz, and Pr Alfred Anwander for helpful discussion and information. *Conflict of Interest*: None declared.

References

Abe M, Hanakawa T. 2009. Functional coupling underlying motor and cognitive functions of the dorsal premotor cortex. Behav Brain Res. 198:13–23.

~~Amft M, Bzdok D, Laird AR, Fox PT, Schilbach L, Eickhoff SB. 2014. Definition and characterization of an extended social-affective default network. Brain Struct Funct. 1–19.~~ Q4

Amiez C, Kostopoulos P, Champod A-S, Petrides M. 2006. Local morphology predicts functional organization of the dorsal premotor region in the human brain. J Neurosci. 26:2724–2731.

Amunts K, Schleicher A, Bürgel U, Mohlberg H, Uylings H, Zilles K. 1999. Broca's region revisited: cytoarchitecture and intersubject variability. J Compar Neurol. 412:319–341.

Behrens TEJ, Johansen-Berg H, Woolrich MW, Smith SM, Wheeler-Kingshott CAM, Boulby PA, Barker GJ, Sillery EL, Sheehan K, Ciccarelli O. 2003. Non-invasive mapping of connections between human thalamus and cortex using diffusion imaging. Nat Neurosci. 6:750–757.

Boussaoud D. 2001. Attention versus intention in the primate premotor cortex. Neuroimage. 14:S40–S45.

Boussaoud D, di Pellegrino G, Wise SP. 1995. Frontal lobe mechanisms subserving vision-for-action versus vision-for-perception. Behav Brain Res. 72:1–15.

Bzdok D, Langner R, Schilbach L, Jakobs O, Roski C, Caspers S, Laird AR, Fox PT, Zilles K, Eickhoff SB. 2013. Characterization of the temporo-parietal junction by combining data-driven

parcellation, complementary connectivity analyses, and functional decoding. Neuroimage. 81:381–392.
Caspers J, Palomero-Gallagher N, Caspers S, Schleicher A, Amunts K, Zilles K. 2015. Receptor architecture of visual areas in the face and word-form recognition region of the posterior fusiform gyrus. Brain Struct Funct. 220:205–219.
Caspers J, Zilles K, Eickhoff SB, Schleicher A, Mohlberg H, Amunts K. 2013. Cytoarchitectonical analysis and probabilistic mapping of two extrastriate areas of the human posterior fusiform gyrus. Brain Struct Funct. 218:511–526.
Caspers S, Eickhoff SB, Geyer S, Scheperjans F, Mohlberg H, Zilles K, Amunts K. 2008. The human inferior parietal lobule in stereotaxic space. Brain Struct Funct. 212:481–495.
Caspers S, Geyer S, Schleicher A, Mohlberg H, Amunts K, Zilles K. 2006. The human inferior parietal cortex: cytoarchitectonic parcellation and interindividual variability. Neuroimage. 33:430–448.
Caspers S, Moebus S, Lux S, Pundt N, Schütz H, Mühleisen TW, Gras V, Eickhoff SB, Romanzetti S, Stöcker T. 2014. Studying variability in human brain aging in a population-based German cohort—rationale and design of 1000BRAINS. Front Aging Neurosci. 6.
Caspers S, Zilles K, Laird AR, Eickhoff SB. 2010. ALE meta-analysis of action observation and imitation in the human brain. Neuroimage. 50:1148–1167.
Cavanna AE, Trimble MR. 2006. The precuneus: a review of its functional anatomy and behavioural correlates. Brain. 129:564–583.
Choi EY, Yeo BT, Buckner RL. 2012. The organization of the human striatum estimated by intrinsic functional connectivity. J Neurophysiol. 108:2242–2263.
Choi HJ, Zilles K, Mohlberg H, Schleicher A, Fink GR, Armstrong E, Amunts K. 2006. Cytoarchitectonic identification and probabilistic mapping of two distinct areas within the anterior ventral bank of the human intraparietal sulcus. J Compar Neurol. 495:53–69.
Chouinard PA, Paus T. 2006. The primary motor and premotor areas of the human cerebral cortex. Neuroscientist. 12:143–152.
Cieslik EC, Zilles K, Caspers S, Roski C, Kellermann TS, Jakobs O, Langner R, Laird AR, Fox PT, Eickhoff SB. 2013. Is there "One" DLPFC in cognitive action control? Evidence for heterogeneity from co-activation-based parcellation. Cerebr Cortex. 23:2677–2689.
Clos M, Amunts K, Laird AR, Fox PT, Eickhoff SB. 2013. Tackling the multifunctional nature of Broca's region meta-analytically: co-activation-based parcellation of area 44. Neuroimage. 83:174–188.
Collette F, Hogge M, Salmon E, Van der Linden M. 2006. Exploration of the neural substrates of executive functioning by functional neuroimaging. Neuroscience. 139:209–221.
Corbetta M, Shulman GL. 2002. Control of goal-directed and stimulus-driven attention in the brain. Nat Rev Neurosci. 3:201–215.
Eickhoff SB, Bzdok D, Laird AR, Kurth F, Fox PT. 2012. Activation likelihood estimation meta-analysis revisited. Neuroimage. 59:2349–2361.
Eickhoff SB, Bzdok D, Laird AR, Roski C, Caspers S, Zilles K, Fox PT. 2011. Co-activation patterns distinguish cortical modules, their connectivity and functional differentiation. Neuroimage. 57:938–949.
Eickhoff SB, Jbabdi S, Caspers S, Laird AR, Fox PT, Zilles K, Behrens TE. 2010. Anatomical and functional connectivity of cytoarchitectonic areas within the human parietal operculum. J Neurosci. 30:6409–6421.
Eickhoff SB, Stephan KE, Mohlberg H, Grefkes C, Fink GR, Amunts K, Zilles K. 2005. A new SPM toolbox for combining probabilistic cytoarchitectonic maps and functional imaging data. Neuroimage. 25:1325–1335.
Eickhoff SB, Thirion B, Varoquaux G, Bzdok D. 2015. Connectivity-based parcellation: critique and implications. Hum Brain Mapp. Q6
Flaugnacco E, Lopez L, Terribili C, Zoia S, Buda S, Tilli S, Monasta L, Montico M, Sila A, Ronfani L, et al. 2014. Rhythm perception and production predict reading abilities in developmental dyslexia. Front Hum Neurosci. 8:392.
Geyer S, Ledberg A, Schleicher A, Kinomura S, Schormann T, Bürgel U, Klingberg T, Larsson J, Zilles K, Roland PE. 1996. Two different areas within the primary motor cortex of man. Q7
Geyer S, Matelli M, Luppino G, Zilles K. 2000. Functional neuroanatomy of the primate isocortical motor system. Anat Embryol. 202:443–474.
Geyer S, Schleicher A, Zilles K. 1999. Areas 3a, 3b, and 1 of human primary somatosensory cortex. Neuroimage. 10:63–83.
Grefkes C, Geyer S, Schormann T, Roland P, Zilles K. 2001. Human somatosensory area 2: observer-independent cytoarchitectonic mapping, interindividual variability, and population map. Neuroimage. 14:617–631.
Grosbras MH, Beaton S, Eickhoff SB. 2012. Brain regions involved in human movement perception: a quantitative voxel-based meta-analysis. Hum Brain Mapp. 33:431–454.
Hanakawa T. 2011. Rostral premotor cortex as a gateway between motor and cognitive networks. Neurosci Res. 70:144–154.
Hanakawa T, Honda M, Sawamoto N, Okada T, Yonekura Y, Fukuyama H, Shibasaki H. 2002. The role of rostral Brodmann area 6 in mental-operation tasks: an integrative neuroimaging approach. Cerebr Cortex. 12:1157–1170.
Hardwick RM, Rottschy C, Miall RC, Eickhoff SB. 2013. A quantitative meta-analysis and review of motor learning in the human brain. Neuroimage. 67:283–297.
Hoshi E. 2013. Cortico-basal ganglia networks subserving goal-directed behavior mediated by conditional visuo-goal association. Front Neural Circuits. 7:158.
Hoshi E, Tanji J. 2007. Distinctions between dorsal and ventral premotor areas: anatomical connectivity and functional properties. Curr Opin Neurobiol. 17:234–242.
Johansen-Berg H, Behrens TEJ, Robson MD, Drobnjak I, Rushworth MFS, Brady JM, Smith SM, Higham DJ, Matthews PM. 2004. Changes in connectivity profiles define functionally distinct regions in human medial frontal cortex. Proc Natl Acad Sci USA. 101:13335–13340.
Kahnt T, Chang LJ, Park SQ, Heinzle J, Haynes J-D. 2012. Connectivity-based parcellation of the human orbitofrontal cortex. J Neurosci. 32:6240–6250.
Kantak SS, Stinear JW, Buch ER, Cohen LG. 2012. Rewiring the brain: potential role of the premotor cortex in motor control, learning, and recovery of function following brain injury. Neurorehabil Neural Repair. 26:282–292.
Kelly C, Toro R, Di Martino A, Cox CL, Bellec P, Castellanos FX, Milham MP. 2012. A convergent functional architecture of the insula emerges across imaging modalities. Neuroimage. 61:1129–1142.
Kelly C, Uddin LQ, Shehzad Z, Margulies DS, Castellanos FX, Milham MP, Petrides M. 2010. Broca's region: linking human brain functional connectivity data and non-human primate tracing anatomy studies. Eur J Neurosci. 32:383–398.
Klein JC, Behrens TE, Robson MD, Mackay CE, Higham DJ, Johansen-Berg H. 2007. Connectivity-based parcellation of human cortex using diffusion MRI: establishing reproducibility,

validity and observer independence in BA 44/45 and SMA/pre-SMA. Neuroimage. 34:204–211.
Laird AR, Eickhoff SB, Kurth F, Fox PM, Uecker AM, Turner JA, Robinson JL, Lancaster JL, Fox PT. 2009. ALE meta-analysis workflows via the brainmap database: progress towards a probabilistic functional brain atlas. Front Neuroinformat 3.
Langner R, Eickhoff SB. 2013. Sustaining attention to simple tasks: a meta-analytic review of the neural mechanisms of vigilant attention. Psychol Bull. 139:870–900.
Langner R, Sternkopf MA, Kellermann TS, Grefkes C, Kurth F, Schneider F, Zilles K, Eickhoff SB. 2014. Translating working memory into action: behavioral and neural evidence for using motor representations in encoding visuo-spatial sequences. Hum Brain Mapp. 35:3465–3484.
Lebedev MA, Wise SP. 2001. Tuning for the orientation of spatial attention in dorsal premotor cortex. Eur J Neurosci. 13:1002–1008.
Luppino G, Rozzi S, Calzavara R, Matelli M. 2003. Prefrontal and agranular cingulate projections to the dorsal premotor areas F2 and F7 in the macaque monkey. Eur J Neurosci. 17:559–578.
Malikovic A, Amunts K, Schleicher A, Mohlberg H, Eickhoff SB, Wilms M, Palomero-Gallagher N, Armstrong E, Zilles K. 2007. Cytoarchitectonic analysis of the human extrastriate cortex in the region of V5/MT+: a probabilistic, stereotaxic map of area hOc5. Cerebr Cortex. 17:562–574.
Matelli M, Luppino G, Rizzolatti G. 1985. Patterns of cytochrome oxidase activity in the frontal agranular cortex of the macaque monkey. Behav Brain Res. 18:125–136.
Matelli M, Luppino G, Rizzolatti G. 1991. Architecture of superior and mesial area 6 and the adjacent cingulate cortex in the macaque monkey. J Compar Neurol. 311:445–462.
Mazziotta J, Toga A, Evans A, Fox P, Lancaster J, Zilles K, Woods R, Paus T, Simpson G, Pike B. 2001. A probabilistic atlas and reference system for the human brain: International Consortium for Brain Mapping (ICBM). Phil Trans R Soc Lond Ser B Biol Sci. 356:1293–1322.
Nee DE, Brown JW, Askren MK, Berman MG, Demiralp E, Krawitz A, Jonides J. 2013. A meta-analysis of executive components of working memory. Cerebr Cortex. 23:264–282.
Nichols T, Brett M, Andersson J, Wager T, Poline J-B. 2005. Valid conjunction inference with the minimum statistic. Neuroimage. 25:653–660.
Nickl-Jockschat T, Rottschy C, Thommes J, Schneider F, Laird AR, Fox PT, Eickhoff SB. ~~2014. Neural networks related to dysfunctional face processing in autism spectrum disorder. Brain Struct Funct. 1–17.~~
Orban P, Doyon J, Petrides M, Mennes M, Hoge R, Bellec P. 2014. The richness of task-evoked hemodynamic responses defines a pseudohierarchy of functionally meaningful brain networks. Cerebr Cortex.
Overy K, Nicolson RI, Fawcett AJ, Clarke EF. 2003. Dyslexia and music: measuring musical timing skills. Dyslexia. 9:18–36.
Petkov CI, O'Connor KN, Benmoshe G, Baynes K, Sutter ML. 2005. Auditory perceptual grouping and attention in dyslexia. Cogn Brain Res. 24:343–354.
Picard N, Strick PL. 2001. Imaging the premotor areas. Curr Opin Neurobiol. 11:663–672.
Rizzolatti G, Luppino G. 2001. The cortical motor system. Neuron. 31:889–901.
Rizzolatti G, Luppino G, Matelli M. 1998. The organization of the cortical motor system: new concepts. Electroencephalogr Clin Neurophysiol. 106:283–296.
Rottschy C, Caspers S, Roski C, Reetz K, Dogan I, Schulz JB, Zilles K, Laird AR, Fox PT, Eickhoff SB. 2013. Differentiated parietal connectivity of frontal regions for "what" and "where" memory. Brain Struct Funct. 218:1551–1567.
Rottschy C, Langner R, Dogan I, Reetz K, Laird AR, Schulz JB, Fox PT, Eickhoff SB. 2012. Modelling neural correlates of working memory: a coordinate-based meta-analysis. Neuroimage. 60:830–846.
Ryali S, Chen T, Padmanabhan A, Cai W, Menon V. 2015. Development and validation of consensus clustering-based framework for brain segmentation using resting fMRI. J Neurosci Methods. 240:128–140.
Schubotz RI, Anwander A, Knösche TR, von Cramon DY, Tittgemeyer M. 2010. Anatomical and functional parcellation of the human lateral premotor cortex. Neuroimage. 50:396–408.
Schubotz RI, von Cramon DY. 2003. Functional–anatomical concepts of human premotor cortex: evidence from fMRI and PET studies. Neuroimage. 20:S120–S131.
Smith EE, Jonides J. 1999. Storage and executive processes in the frontal lobes. Science. 283:1657–1661.
Tomassini V, Jbabdi S, Klein JC, Behrens TEJ, Pozzilli C, Matthews PM, Rushworth MFS, Johansen-Berg H. 2007. Diffusion-weighted imaging tractography-based parcellation of the human lateral premotor cortex identifies dorsal and ventral subregions with anatomical and functional specializations. J Neurosci. 27:10259–10269.
Wang J, Yang Y, Fan L, Xu J, Li C, Liu Y, Fox PT, Eickhoff SB, Yu C, Jiang T. 2015. Convergent functional architecture of the superior parietal lobule unraveled with multimodal neuroimaging approaches. Hum Brain Mapp. 36:238–257.
Wise SP. 1985. The primate premotor cortex: past, present, and preparatory. Annu Rev Neurosci. 8:1–19.
Yeo BTT, Krienen FM, Sepulcre J, Sabuncu MR, Lashkari D, Hollinshead M, Roffman JL, Smoller JW, Zöllei L, Polimeni JR. 2011. The organization of the human cerebral cortex estimated by intrinsic functional connectivity. J Neurophysiol. 106:1125–1165.
Zago L, Pesenti M, Mellet E, Crivello F, Mazoyer B, Tzourio-Mazoyer N. 2001. Neural correlates of simple and complex mental calculation. Neuroimage. 13:314–327.

I. Supplemental methods

I.1. VOI definition

Comparison of our caudal and inferior PMd borders with previous borders

Of note, the inferior border of our meta-analytic definition of the PMd, that is, approximately z = 40 in conventional Montreal Neurological Institute (MNI) space, co-localized in a range of 10 mm with a previously meta-analytically defined border [approximately z = 30; (Mayka et al. 2006)]. Furthermore, our border co-localized with previous PDT-based borders [approximately z = 48 in MNI space by Tomassini et al. (2007) and approximately z = 52 in Talairach space on the right side by Schubotz et al. (2010)].

I.2. MACM selection of experiments

From this database, only experiments using functional Magnetic Resonance Imaging (fMRI) or perfusion positron emission tomography in healthy adults participants without any external interventions (such as pharmacological challenges) were included in the analyses. These inclusion criteria resulted in about 7,500 eligible experiments at the time of analysis.

I.3. ALE for MACM-CBP

The key idea behind ALE is to treat the foci reported in the associated experiments not as single points but as centers for 3-D Gaussian probability distributions that reflect the spatial uncertainty associated with neuroimaging results. For each experiment, the probability distributions of all reported foci were combined into a modeled activation map for that particular experiment (Turkeltaub et al. 2012). The voxel-wise union across the modeled activation maps of all experiments associated with a particular seed voxel then yielded an ALE score for each voxel of the brain. This ALE score describes the co-activation probability of that particular location with the current seed voxel. For each

seed voxel, this computation was performed for all voxels within brain grey matter (based on 10 % probability of finding grey matter according to ICBM).

I.4. k-means clustering

k-means clustering is a non-hierarchical clustering method based on an iterative algorithm. It can be used to divide a VOI into *k* non-overlapping clusters (Hartigan and Wong 1979). Clustering using the *k*-means algorithm consists of minimizing the variance within clusters and maximizing the variance between clusters by first computing the centroid of each cluster and subsequently reassigning voxels to the clusters such that their difference from the nearest centroid is minimal.

I.5. Selection of the optimal filter range

In the present study, the filter range with the lowest number of deviants (i.e., voxels that were assigned differently as compared to the solution from the majority of filters) was selected. The proportion of deviants (normalized within each cluster solution k) is illustrated in Figure S1. We observed the same profile like in (Clos et al. 2013). That is, parcellations based on small as well as large filter sizes yielded more deviants. The enlargement of the filter size refers to a more liberal inclusion of experiments in term of spatial distance for each seed voxel. It results in greater smoothness of the data. Larger filter size may result in the spatial spectrum of the voxels becoming actually higher than the actual spatial resolution of the clusters. It would therefore potentially result in more arbitrary cluster borders. Thus, the filter size range chosen (85 to 145) was based on the increase in the weighted sum (across all k) of the z-normalized number of deviants before and after these filter size values (cut off at $z < -0.5$: only those filter sizes were included where the number of deviants was at least half a standard deviation lower than the average number of deviants across all filter sizes). This filter size range corresponds to an effective distance ranging between 6 and 8 mm or between 3 and 4 voxels.

[Figure S1 about here]

I.6. Selection of the optimal clustering solution

In line with previous CBP studies (Kelly et al. 2010; Kahnt et al. 2012; Kelly et al. 2012; Clos et al. 2013), we considered information-theoretic characteristics of the respective cluster solution. Variation of information (VI) is an information-theoretic measure that quantifies the distance between two clustering solutions in terms of the information gained and lost in choosing one solution over another (Meilă 2007). For each cluster solution, VI between all (unique) combinations of the 13 (85,90,95…145) filter sizes previously selected was computed. A significant difference in VI between a given clustering step and the next clustering step was tested with a two-sample t-test. Solutions were considered stable if no significant increase in VI from the previous to the current clustering step could be observed.

Next, we considered a consistency criterion. For each cluster solution, the average percentage of voxels for each filter size that were assigned to a different cluster compared to the most frequent (mode) assignment of these voxels across filter sizes (i.e., the percentage of deviants or "misclassified voxels") was computed. A significant difference in percentage of deviants between a given cluster solution and the previous one was tested using a two-sample t-test. In this framework, optimal solutions are those k parcellations where the percentage of deviants (presumably reflecting noise and local variance) is not significantly increased compared to the previous (k-1) solution, while the subsequent (k+1) solution leads to a significantly higher percentage of deviants.

Third, separation characteristics were also taken into account in determining the best cluster solution. As done in previous CBP studies (Kelly et al. 2010; Cauda et al. 2012), for each cluster solution, the silhouette value averaged across voxels for each filter in the previously selected range was computed. The silhouette value is a measure ranging from -1 to 1. It assesses, for each voxel, how similar the voxel is to others within the same cluster, versus, how similar this voxel is to voxels in other clusters regarding co-activation profile. A significant difference in the silhouette value between a given cluster solution and the previous one was tested with a two-sample t-test. Cluster solutions were considered favorable if they show a significantly higher silhouette value, as compared to the previous (k-1) solution (primary criterion), or if they did not show a significantly lower silhouette value than the previous cluster solution (secondary criterion).

[Figure S2 about here]

As illustrated in Figure S2, the above criteria identified a 5-cluster (5k) solution as the most stable parcellation of the right PMd. First, the VI across filters showed that there is no significant increase in VI from the 4k to the 5k solution, whereas a significant increase in VI was observed between the 5k and the 6k solution (Figure S2A). Second, the percentage of "misclassified voxels" (deviants) did not significantly increase from the 4k to the 5k solution, whereas it increased significantly from the 5k to the 6k solution (Figure S2B). Finally, the silhouette value indicated that the 5k solution led to one of the best voxel pattern separations (Figure S2C).

Notably, no voxel appeared to be spatially inconsistent in the 5k solution, that is, all 5 clusters were formed of contiguous voxels.

I.7. Acquisition and preprocessing of RSFC data and time series computation

From each participant, echo-planar Imaging (EPI) images were obtained at rest (participants were instructed to keep their eyes closed and to think about nothing in particular but not to fall asleep) during 11 minutes (±300 scans). These images were acquired with a Siemens TIM Trio 3-T scanner using Blood-Oxygen-Level Dependent (BOLD) contrast [gradient-echo EPI pulse sequence, TR = 2.2 s, echo time, TE = 30 ms, flip angle = 90°, 36 axial slices (3.1mm thickness), covering the entire brain].

EPI images were corrected for head movements by affine registration. This was achieved by using a two-pass procedure in which the images were first aligned to the initial volumes and subsequently to the mean. The mean EPI image for each participant was then spatially normalized to the Montreal Neurological Institute (MNI) single-subject template using the "unified segmentation" approach (Ashburner and Friston 2005). The ensuing deformation was then applied to the individual EPI volumes.

The time-series data of each voxel were adjusted in order to remove sources of artificial and confounding signals and hence reduce spurious correlations. To do so, we first performed a PCA denoising (cf. (Behzadi et al., 2007 & Soltysk et al., 2014)). That is, we computed a principal component analysis (PCA) decomposition across the WM and CSF regions of the brain and then removed variance associated with the most dominant 5 components. Furthermore, variance that could be explained by the following nuisance

variables was removed (cf. Satterthwaite et al. 2013 for an evaluation of this framework): 1) the 6 motion parameters derived from the image realignment; 2) their first derivatives; 3) global signal (as average across all voxels at each time-point). Finally, data was band-pass filtered with the cut-off frequencies of 0.01 and 0.08 Hz.

I.8. ALE for MACM of the derived cluster

Main effect

To establish which regions were significantly co-activated with a given cluster, ALE scores for the MACM analysis of the respective cluster were compared with a null-distribution. This null-distribution reflects a random spatial association between experiments with a fixed within-experiment distribution of foci (Eickhoff et al. 2009; Eickhoff et al. 2012). This random-effects inference assesses above-chance convergence between experiments, not between clustering of foci within a particular experiment. The observed ALE scores from the actual meta-analysis of experiments activating within a particular cluster were then tested against the ALE scores obtained under the null-distribution of random spatial association between experiments.

Contrasts

The null-distributions were derived by first pooling all experiments contributing to either analysis (i.e., the two MACM results of the clusters to be compared, respectively) and then randomly divided into two groups of the same size as the two original sets of experiments defined by activation in the first or second cluster (Eickhoff et al. 2011). ALE scores for these two randomly assembled groups were calculated and the difference between these ALE scores was recorded for each voxel. Repeating this process 25,000 times yielded a null-distribution of differences in ALE scores between the MACM analyses of the two clusters. The “true” difference in ALE scores was then tested against this null-distribution.

II. Supplemental results

II.1. Visualization of splitting in functional space

As done previously (Cauda et al. 2012; Clos et al. 2013), we used multidimensional scaling (MDS) to visualize the succession of cluster separation/splitting. The pattern of connectivity of each voxel is a multidimensional dataset (N-dimensional functional space) that can be better visualized using algorithms involving a dimensional reduction to 2D. Thus, we performed MDS on the eigenimage of the distance matrices using Sammon's nonlinear mapping as the goodness-of-fit criterion. In the MDS representation, voxels featuring a similar pattern of whole-brain co-activation probabilities are placed together in this visualization, while voxels having dissimilar patterns of whole-brain co-activations are placed further apart. The splittings of the five clusters into functional space (2-D visualization) across the different cluster solutions (from k = 2 to k = 5) is shown in Figure S3A. This representation in functional space illustrates how the right PMd voxels can be successively clustered according to their functional co-activation profile into two clusters (k = 2), then three clusters (k = 3), four clusters (k = 4) and finally five clusters (k = 5). It therefore illustrates how a child cluster emerged from the parent cluster(s). At k = 2, the right PMd could be divided into a posterior (caudal) and an anterior (rostral) cluster. At the next level (k = 3), a third (central) cluster emerged from both the anterior and posterior cluster. At the following step (k = 4), the posterior and anterior clusters remained the same but a fourth cluster emerged mainly from the central cluster. This fourth cluster was further split into two parts at the last clustering step.

[Figure S3 about here]

II.2. Borders of MACM-CBP-derived clusters

On the y-axis, the border between the rostral and central clusters lies approximately between y = 0 and y = 5, while between the central and caudal clusters it lies approximately between y = -7 and y = -14. On the z-axis, the border between the ventral and central/rostral clusters lies between z = 50 and z = 60, while the borders between the central/rostral and dorsal clusters lies approximately at z = 70.

II.3. Overlap between 5k MACM-CBP and 5k from other modalities

To roughly quantify the agreement of both parcellation into 5 clusters of our PMd VOI, we computed the number of overlapping voxels in each pair of clusters as reflected by a min(X) conjunction. This procedure revealed a major overlap between the MACM-CBP-derived 5k and the PDT-CBP-derived 5k spatial pattern and a decent overlap between the former and the RSFC-CBP-derived pattern (see Table S1).

Table S1. Overlap between MACM-CBP-derived clusters and the respective PDT and RSFC –CBP-derived clusters expressed as numbers of voxels.

MACM-CBP-derived cluster (number of voxels)	PDT-CBP	RSFC-CBP
Rostral (1035)	866	508
Caudal (784)	720	559
Central (1049)	889	329
Ventral (685)	666	404
Dorsal (590)	547	455
Total (4143)	3688 (89%)	2255 (55%)

III. Supplemental discussion

III.1. Methodological considerations

III.1.1. Task-based functional definition of the VOI

Our functional definition of the PMd was based on meta-analytic approach of fMRI and PET activation studies. However, nearly all fMRI studies require hand or eye movements in relation to stimuli. Therefore, our functional definition may have been biased toward a hand/finger functional definition. That is, it may have failed to capture the medial and posterior extremity of BA6 extending to M1, which is likely related to lower limb movements (e.g. Cauda et al. 2011). Nevertheless, while a somatotopy is relatively obvious in primary sensorimotor areas in activation studies, a foot/leg functional subregion in the PMd appears to be less supported by such studies (e.g. Rijntjes et al. 1999). Therefore, the empirical evidence supporting this hypothesis are still lacking and further studies should address this issue.

III.1.2 Divergence between MACM and RSFC characterizing the FC pattern of the clusters

We generally found a good convergence in the specific pattern of functional connectivity of each cluster as revealed by MACM and RSFC suggesting that each cluster has a robust functional specific connectivity fingerprint. However, some cluster's specific functional connectivity were only revealed by one modality. In general, RSFC showed more coarse functional connectivity profiles, which may spatially gather distinct behaviorally functionally specialized lobules (such as the primary somatosensory cortex and the supramarginal gyrus). This pattern of larger spatial smoothness mirrors and extents observations from previous multi-modal connectivity studies (cf. Hardwick et al. 2015, Clos et al., 2014). Whether it is indeed physiological (reflecting a broader recruitment as in the arguably more specifically focused task-state) or resulting from technical/methodological aspects remains unclear. In contrast, MACM showed more restricted functional connectivity profile. However, as reflecting co-activation of voxels during tasks, MACM may be influenced by the experimental settings. That is, some aspects of the profile provided by MACM may be potentially driven by some epiphenomena that may be universal in task-based fMRI and PET studies such as "hand-eye" functional coupling. Nevertheless, in the present study, MACM allowed highlighting

that our ventral cluster was specifically functionally coupled with the visual cortex (which is congruent with the behavioral functional decoding of this former). Such coupling may be specific to the engagement in behavioral task and thus may not be consistently evidenced by functional connectivity at rest, when subjects lie, eyes closed, in the scanner and let their mind wandering. Thus, despite the limitations of MACM should be taken in mind when addressing spatial functional organization of the brain (such as in CBP issue), in the present study, MACM specifically revealed that the ventral cluster is functionally connected to the visual cortex.

III.1.3. Potential limitations of MACM-CBP

Is the central cluster an artifact of MACM-CBP?

Our parcellation of the right PMd is primarily based on MACM, which is a quantitative approach of functional activations studies. The parcellation yielded by MACM-CBP relies on average of group's peaks of activations of thousands of fMRI and PET studies. The co-activation profile of each seed voxel is estimated by the ALE method averaging peaks of thousands of group studies. Consequently, one may hypothesized that some voxels, located at a spatial border between two clearly distinct functional regions, may show a mixed, undefined profile. According to this speculation, clustering and functional characterization may reveal an intermediate cluster, showing an unspecified behavioral profile, as the central one observed in the current study. In contrast, RSFC-CBP and PDT-CBP are both based on unique sample of subjects whose data have been acquired and preprocessed with similar settings and procedure. While PDT-CBP is based on diffusion data of a sample of regular size of subject in whom the connectivity profile of each seed voxel is estimated by probabilistic tractography, RSFC-CBP is based on behaviorally unconstrained functional data of a big sample of subjects in whom the connectivity profile of each seed voxel is estimated by correlation between time series. In both CBP approaches, the voxels are then clustered according to their connectivity profile at the subject level. Then, for each cluster's solution, the convergence across subjects is obtained by computing a maximum probability map. Despite these CBP approaches may suffer form spatial uncertainty resulting in spurious clusters at the subject level, the computation of intersubject should help to prevent such biais at the group level. Thus, in summary, whereas the parcellation of the VOI is performed following averaging of

group's peaks with MACM-CBP, this parcellation is performed for each subject and then validated at the group level in PDT-CBP. Consequently, PDT-CBP and RSFC-CBP are less likely to result in the emergence of spurious intermediate clusters. In the present study, both, PDT-CBP and RSFC-CBP, support the existence of a centrally located cluster suggesting that this latter is not an artifact driven by spatial uncertainty inherent to MACM.

Further evidence against the hypothesis of the central cluster being an artifact of MACM-CBP (or even any CBP approach) may also be found in the follow-up analysis of the derived clusters. Indeed, if the emergence of the central cluster were an artifact resulting from poor spatial resolution, the statistical comparison of the connectivity profile of this cluster with the connectivity profiles of the other clusters would likely have yielded a null result. Hence, statistical comparisons allowed highlighting a connectivity profile whose specificity to the central cluster is significant. Finally, if the emergence of a central cluster were driven by the methods employed, previous parcellations based on similar methods would have revealed a similar pattern, but they did not (e.g. Bzdok et al., 2013, Cieslik et al., 2013, Eickhoff et al., 2014, Bzdok et al., 2015). To our knowledge, our parcellation of the right PMd is the first MACM-CBP study revealing a central cluster.

Functional propinquity of the ventral and dorsal clusters

When comparing the different cluster solutions, the splitting order towards more clusters shows that a ventral and a dorsal subregion jointly emerged as one cluster from the central one. That is, the comparison of functional and spatial space suggests that the spatially distant ventral and dorsal clusters could form a single cluster at k = 4 based on the similarity of the respective co-activation profiles. In this issue, it is important to remember that the algorithm clusters voxels only according to the similarity of their co-activation profile without any regards to their location in the brain. This may result in two spatially distant voxels being clustered together because they show similar co-activation profile. As MACM relies on task functional connectivity, the clustering based on MACM is constrained by the tasks used in fMRI experiments. That may result in voxels being clustered together not because of any biological constraints but rather

because of experimental functional constraints. For example, voxels engaged in eye movements and voxels engaged in hand movements may be likely to be clustered together because they are frequently co-activated across a range of behavioral tasks. In the present study, additional support for the distinction of the ventral and dorsal subregions has been provided by examination of the 5k revealed PDT-CBP and RSFC-CBP. In particular, PDT-CBP showed that the ventral and dorsal clusters may be distinguished based on their structural connectivity profiles. Thus, in the present study, examining different CBP modalities highlighted the robustness of the topographical pattern revealed by MACM-CBP.

In the same vein, following functional decoding, the ventral and dorsal clusters were both related to action execution, suggesting that both clusters play a role in motor functions. However, the functional profiles of the ventral and dorsal clusters also showed significant differences. While the ventral cluster was more strongly associated with eye movements/visual attention, the dorsal one was more strongly related to finger tapping.

III.2. Theoretical considerations

III.2.1. Functional connectivity between the ventral cluster and posterior temporal cortex

Somewhat surprisingly, functional connectivity analyses revealed that the ventral cluster was functionally coupled with the right posterior middle/superior temporal cortex. This region, however, has been demonstrated to be engaged in face processing (Fusar-Poli, Placentino, Carletti, Allen, et al. 2009; Fusar-Poli, Placentino, Carletti, Landi, et al. 2009), particularly in gaze processing (Carlin and Calder 2013), as well as in emotional scene processing (Sabatinelli et al. 2011). This suggests that this posterior superior temporal region might play a role in interpretation of visual cues. One may assume that the process required in the processing of faces and emotional scenes and supported by our ventral cluster is the engagement of eye movements for visual scanning.

III.2.2 Two potential eye-field candidates

The location of the FEF has been debated for long. Amiez and Petrides's (2009) review and empirical work has highlighted two potential eye-fields in humans: the superior precentral sulcus eye field (SP-EF) and the inferior precentral sulcus eye field (IP-EF). The SP-EF is located in the ventral branch of the superior precentral sulcus (MNI coordinates: y = -9.4, z = 54.4). Roughly, the SP-EF corresponds to the FEF, as suggested by activation studies in humans (Paus, 1996). That is, activations related to saccades and more complex eye-related functions have been usually found at the intersection of the superior precentral sulcus (SPS) and the superior frontal sulcus (SFS). The IP-EF has been also called "premotor eye field". It is located in the dorsal branch of the inferior precentral sulcus (MNI coordinates y = -3.9, z = 44). This premotor eye-field shows anatomical correspondence with the eye blink area suggested by Kato and Miyauchi (2003a, 2003b)*. Thus, altogether, previous work suggests that two potential eye-fields may be found in the precentral sulcus: a more superior one (SP-EF) showing activations for eye-related processes, and a more inferior or ventral one (IP-EF) showing activations for blinking and corresponding to the eye field evidenced by stimulation studies.

Along the same lines, our quantitative approach of activation studies highlighted two potential eye-fields as defined by activations for saccade/antisaccade paradigms: the central cluster and the ventral cluster. An anatomical comparison suggests that while our central cluster overlaps with the SP-EF, our ventral cluster rather overlaps with the IP-EF. Similarly, a comparison of Kato and Miyauchi's (2003) findings with our clusters showed that saccades are related to activation in both the central cluster (MNI peak coordinates: 24 -9 47) and the ventral cluster (MNI peak coordinates: 44 -0.2 48). In contrast, blinking activates only the inferior part of our ventral cluster (MNI peak coordinates: 51.5 -4 44.4). Therefore, overall, these findings suggest that whereas both the central and ventral clusters may be activated during saccades in fMRI studies and thus considered as potential eye-field, only the ventral cluster shows additional activation for "basic" eye-related functions like blinking, as well as a broader association with the domain of vision.

*Note 1: Please note that the similarities between the premotor eye field and the eye blink area may suggest that the inferior part of the PMd is engaged in eye-movements, but also, more generally in upper face movements, such as eyelid movements.

III.2.3. Two functional labels corresponding to the central cluster

According to its spatial location and its functional pattern, the central cluster could be related to two functional concepts: F2vr and SP-EF. Whereas F2vr has been suggested by studies in non-human primates (for a review see Abe M and T Hanakawa 2009), SP-EF has been proposed by Amiez and Petrides (2009) following a review comparing findings in non-human primates with activations studies in humans. Despite these two concepts have not been comprehensively examined in the previous literature, from a functional point of view, one may assume that those two concepts actually refer to one functional module. One may indeed expect a functional module as F2vr to be engaged in a broad range of visuo-spatio-motor functions including saccades characterizing SP-EF. We therefore assume that F2vr and SP-EF are two concepts referring to an unique functional module localized in the central cluster in the present study.

III.2.4. A dynamic functional mosaic within the right PMd

In a dynamic (i.e. not perceptually static) and complex environment, a sustained (i.e. constant) integration of cognitive, spatial, and multimodal sensory representations with (perceptually guided) motor commands is required. The present study has shown that these representations and their related processes may be neuroanatomically organized in a mosaic of five functionally distinct parts within the right PMd. In the framework of goal-directed behavior, recent studies suggest that lateral prefrontal regions support the maintenance of abstract goals (Hoshi 2013). These regions interact with the rostral PMd, which maintains visuospatial cues related to the goals (Hoshi et al., 2013). Our study further suggests that this “cognitive” rostral part, in turn, interacts with the core/central cluster, which coordinates cognitive information with motor programming supported by the caudal PMd. Our study also suggests that the central cluster may integrate maintained cognitive information and motor programming with eye-related processes (such as eye position or visual scanning of the environment) supported by the ventral cluster. Finally, we showed that the caudal cluster interacts with a wide sensorimotor network to control action execution.

References

Amiez C, Petrides M. 2009. Anatomical organization of the eye fields in the human and non-human primate frontal cortex. Progress in neurobiology 89:220-230.
Ashburner J, Friston KJ. 2005. Unified segmentation. NeuroImage 26:839-851.
Carlin JD, Calder AJ. 2013. The neural basis of eye gaze processing. Curr Opin Neurobiol 23:450-455.
Cauda F, Costa T, Torta DM, Sacco K, D'Agata F, Duca S, Geminiani G, Fox PT, Vercelli A. 2012. Meta-analytic clustering of the insular cortex: characterizing the meta-analytic connectivity of the insula when involved in active tasks. Neuroimage 62:343-355.
Cauda F, Geminiani G, D'Agata F, Duca S, Sacco K. 2011. Discovering the somatotopic organization of the motor areas of the medial wall using low‐frequency bold fluctuations. Human brain mapping 32:1566-1579.
Clos M, Amunts K, Laird AR, Fox PT, Eickhoff SB. 2013. Tackling the multifunctional nature of Broca's region meta-analytically: co-activation-based parcellation of area 44. NeuroImage 83:174-188.
Eickhoff SB, Bzdok D, Laird AR, Kurth F, Fox PT. 2012. Activation likelihood estimation meta-analysis revisited. NeuroImage 59:2349-2361.
Eickhoff SB, Bzdok D, Laird AR, Roski C, Caspers S, Zilles K, Fox PT. 2011. Co-activation patterns distinguish cortical modules, their connectivity and functional differentiation. NeuroImage 57:938-949.
Eickhoff SB, Laird AR, Grefkes C, Wang LE, Zilles K, Fox PT. 2009. Coordinate‐based activation likelihood estimation meta‐analysis of neuroimaging data: A random‐effects approach based on empirical estimates of spatial uncertainty. Human brain mapping 30:2907-2926.
Fusar-Poli P, Placentino A, Carletti F, Allen P, Landi P, Abbamonte M, Barale F, Perez J, McGuire P, Politi P. 2009. Laterality effect on emotional faces processing: ALE meta-analysis of evidence. Neuroscience letters 452:262-267.
Fusar-Poli P, Placentino A, Carletti F, Landi P, Allen P, Surguladze S, Benedetti F, Abbamonte M, Gasparotti R, Barale F, Perez J, McGuire P, Politi P. 2009. Functional atlas of emotional faces processing: a voxel-based meta-analysis of 105 functional magnetic resonance imaging studies. Journal of psychiatry & neuroscience : JPN 34:418-432.
Hartigan JA, Wong MA. 1979. Algorithm AS 136: A k-means clustering algorithm. Journal of the Royal Statistical Society Series C (Applied Statistics) 28:100-108.
Hoshi E. 2013. Cortico-basal ganglia networks subserving goal-directed behavior mediated by conditional visuo-goal association. Frontiers in neural circuits 7:158.
Kahnt T, Chang LJ, Park SQ, Heinzle J, Haynes J-D. 2012. Connectivity-based parcellation of the human orbitofrontal cortex. The Journal of Neuroscience 32:6240-6250.
Kato M, Miyauchi S. 2003a. Functional MRI of brain activation evoked by intentional eye blinking. Neuroimage 18:749-759.
Kato M, Miyauchi S. 2003b. Human precentral cortical activation patterns during saccade tasks: an fMRI comparison with activation during intentional eyeblink tasks. Neuroimage 19:1260-1272.
Kelly C, Toro R, Di Martino A, Cox CL, Bellec P, Castellanos FX, Milham MP. 2012. A convergent functional architecture of the insula emerges across imaging modalities. NeuroImage 61:1129-1142.
Kelly C, Uddin LQ, Shehzad Z, Margulies DS, Castellanos FX, Milham MP, Petrides M. 2010. Broca’s region: linking human brain functional connectivity data and non-human primate tracing anatomy studies. European Journal of Neuroscience 32:383-398.

Mayka MA, Corcos DM, Leurgans SE, Vaillancourt DE. 2006. Three-dimensional locations and boundaries of motor and premotor cortices as defined by functional brain imaging: a meta-analysis. Neuroimage 31:1453-1474.
Meilă M. 2007. Comparing clusterings—an information based distance. Journal of Multivariate Analysis 98:873-895.
Rijntjes M, Dettmers C, Büchel C, Kiebel S, Frackowiak RSJ, Weiller C. 1999. A blueprint for movement: functional and anatomical representations in the human motor system. The Journal of neuroscience 19:8043-8048.
Sabatinelli D, Fortune EE, Li Q, Siddiqui A, Krafft C, Oliver WT, Beck S, Jeffries J. 2011. Emotional perception: meta-analyses of face and natural scene processing. Neuroimage 54:2524-2533.
Satterthwaite TD, Elliott MA, Gerraty RT, Ruparel K, Loughead J, Calkins ME, Eickhoff SB, Hakonarson H, Gur RC, Gur RE, Wolf DH. 2013. An improved framework for confound regression and filtering for control of motion artifact in the preprocessing of resting-state functional connectivity data. Neuroimage 64:240-256.
Schubotz RI, Anwander A, Knösche TR, von Cramon DY, Tittgemeyer M. 2010. Anatomical and functional parcellation of the human lateral premotor cortex. NeuroImage 50:396-408.
Tomassini V, Jbabdi S, Klein JC, Behrens TEJ, Pozzilli C, Matthews PM, Rushworth MFS, Johansen-Berg H. 2007. Diffusion-weighted imaging tractography-based parcellation of the human lateral premotor cortex identifies dorsal and ventral subregions with anatomical and functional specializations. The Journal of neuroscience 27:10259-10269.
Turkeltaub PE, Eickhoff SB, Laird AR, Fox M, Wiener M, Fox P. 2012. Minimizing within‐experiment and within‐group effects in activation likelihood estimation meta‐analyses. Human brain mapping 33:1-13.

Figures:

Figure S1. MACM-CBP: deviants and stability. z-scores on median- filtered deviants (normalized for k). The vertical lines specify the ultimately selected, most stable range of filter sizes (i.e., range with least deviants across k). (A) The proportion of deviants computed across filter sizes. Warm/cold colors indicate high/low numbers of deviants. (B) Maximum z- score of median-filtered deviants.

Figure S2. MACM-CBP: cluster solution criteria. (A) Variation of Information (VI) between filter sizes across the 10 cluster solutions; *Significant increase in VI from the previous (k-1) to current (k) cluster solution. (B) Percentage of deviants (misclassified voxels) across the 10 cluster solutions; *Significant increase in percentage of deviants between k- 1 and k. (C) Average silhouette value across cluster solutions; *Significant increase in silhouette value from the previous (k-1) to current (k) cluster solution.

Figure S3. (A) MACM-CBP: Visualization of the five clusters' emergence in functional space by multidimensional scaling across the different cluster solutions (from k = 2 to k

= 5). (B) MACM-CBP: Coronal view of each cluster (upper part); CG: center of gravity (coordinates refer to Montreal Neurological Institute space); Nvox: Number of voxels included in the cluster. Color code: red = rostral cluster, green = caudal cluster, blue = central cluster, yellow = ventral cluster, light blue = dorsal cluster.

Figure S4. Between-clusters contrasts across behavioral domains and paradigm classes significantly associated with each cluster. In that context, “baserate” demotes the a-priori probability of any focus to lie in either of the two compared clusters. A) Contrast between rostral (red) and caudal (green) clusters. B) Contrast between rostral (red) and central (dark blue) clusters. C) Contrast between rostral (red) and ventral (yellow) clusters. D) Contrast between rostral (red) and dorsal (light blue) clusters. E) Contrast between caudal (green) and central (dark blue) clusters. F) Contrasts between caudal (green) and ventral (yellow) clusters. G) Contrasts between caudal (green) and dorsal (light blue) clusters. H) Contrasts between central (dark blue) and ventral (yellow) clusters. I) Contrasts between central (dark blue) and dorsal (light blue) clusters. J) Contrast between ventral (yellow) and dorsal (light blue) clusters.

Figure S1

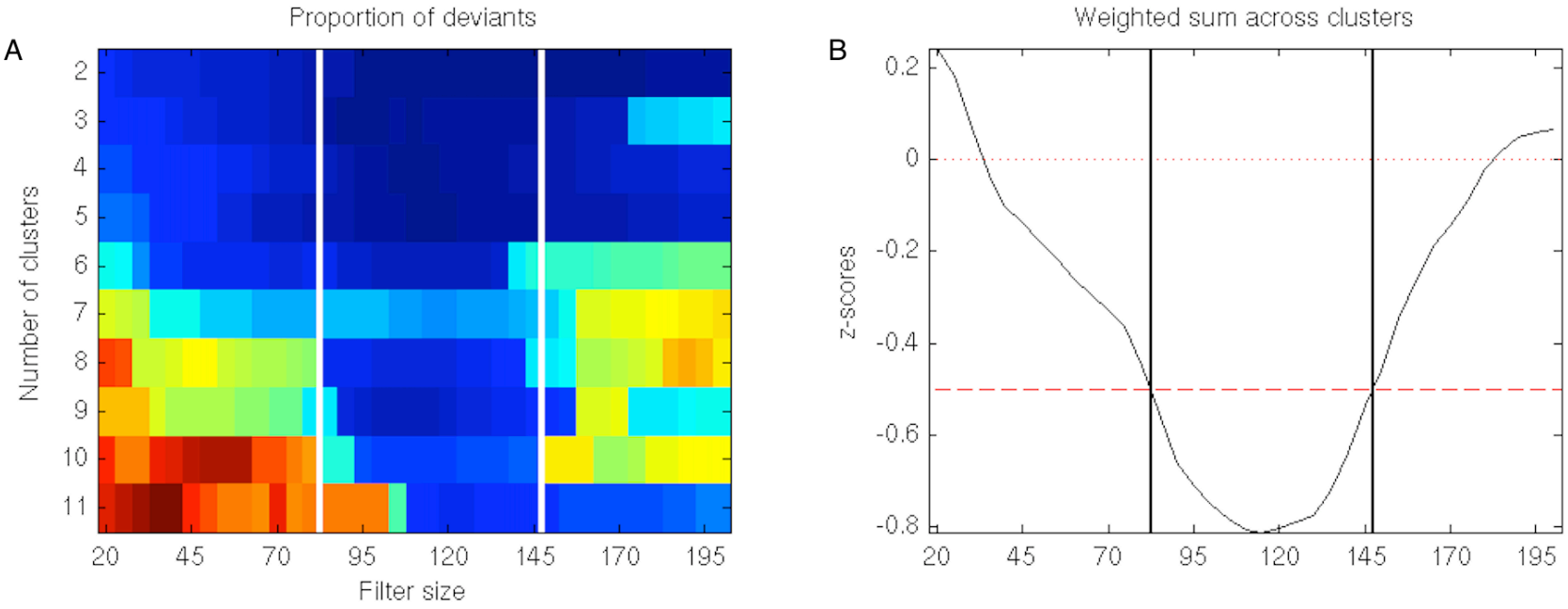
A
Proportion of deviants
Number of clusters
2
3
4
5
6
7
8
9
10
11
20
45
70
95
120
145
170
195
Filter size
B
Weighted sum across clusters
z-scores
0.2
0
-0.2
-0.4
-0.6
-0.8
20
45
70
95
120
145
170
195

Figure S2

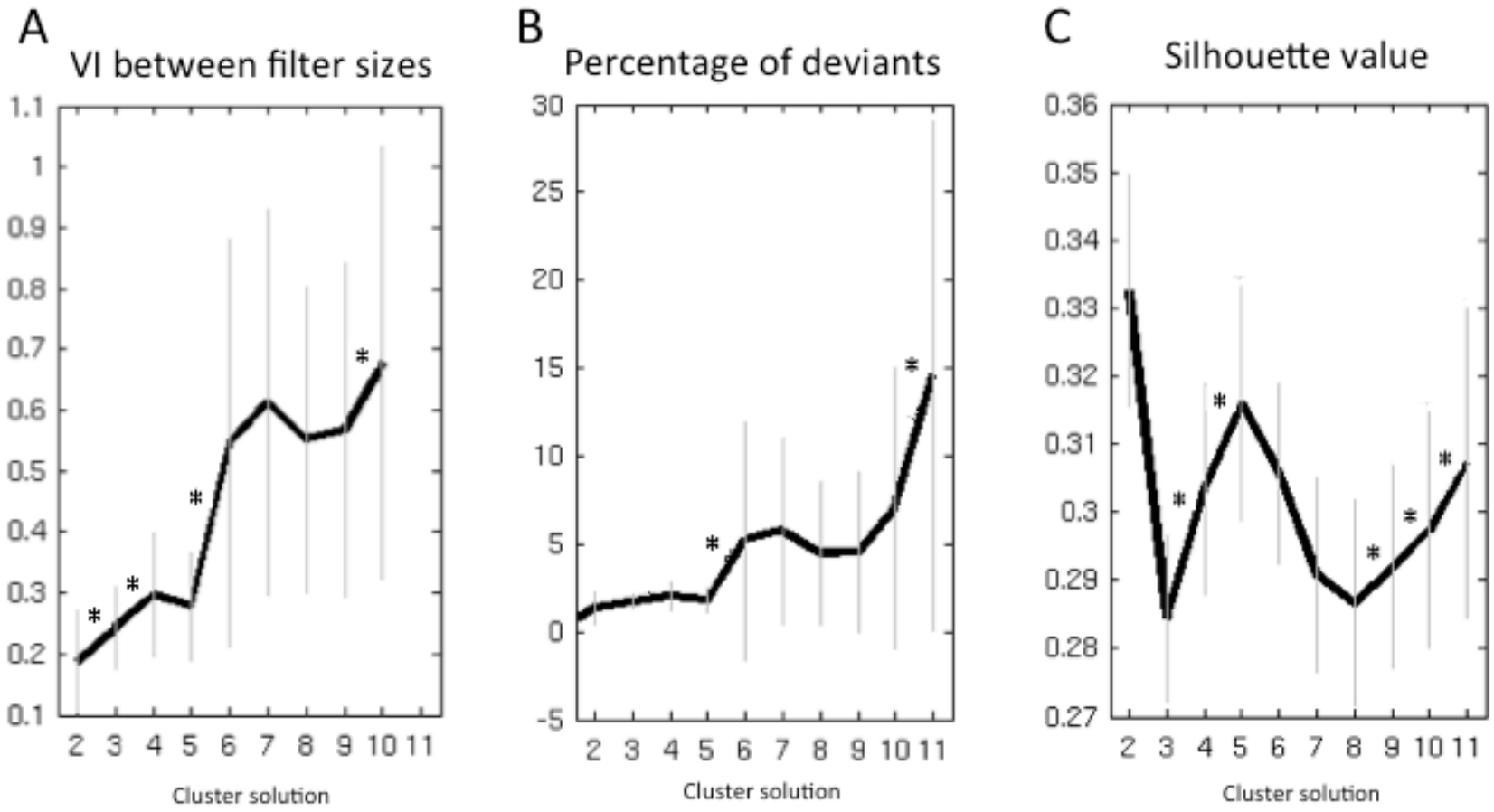
A
VI between filter sizes
1.1
1
0.9
0.8
0.7
0.6
0.5
0.4
0.3
0.2
0.1
2 3 4 5 6 7 8 9 10 11
Cluster solution
B
Percentage of deviants
30
25
20
15
10
5
0
-5
2 3 4 5 6 7 8 9 10 11
Cluster solution
C
Silhouette value
0.36
0.35
0.34
0.33
0.32
0.31
0.3
0.29
0.28
0.27
2 3 4 5 6 7 8 9 10 11
Cluster solution

Figure S3

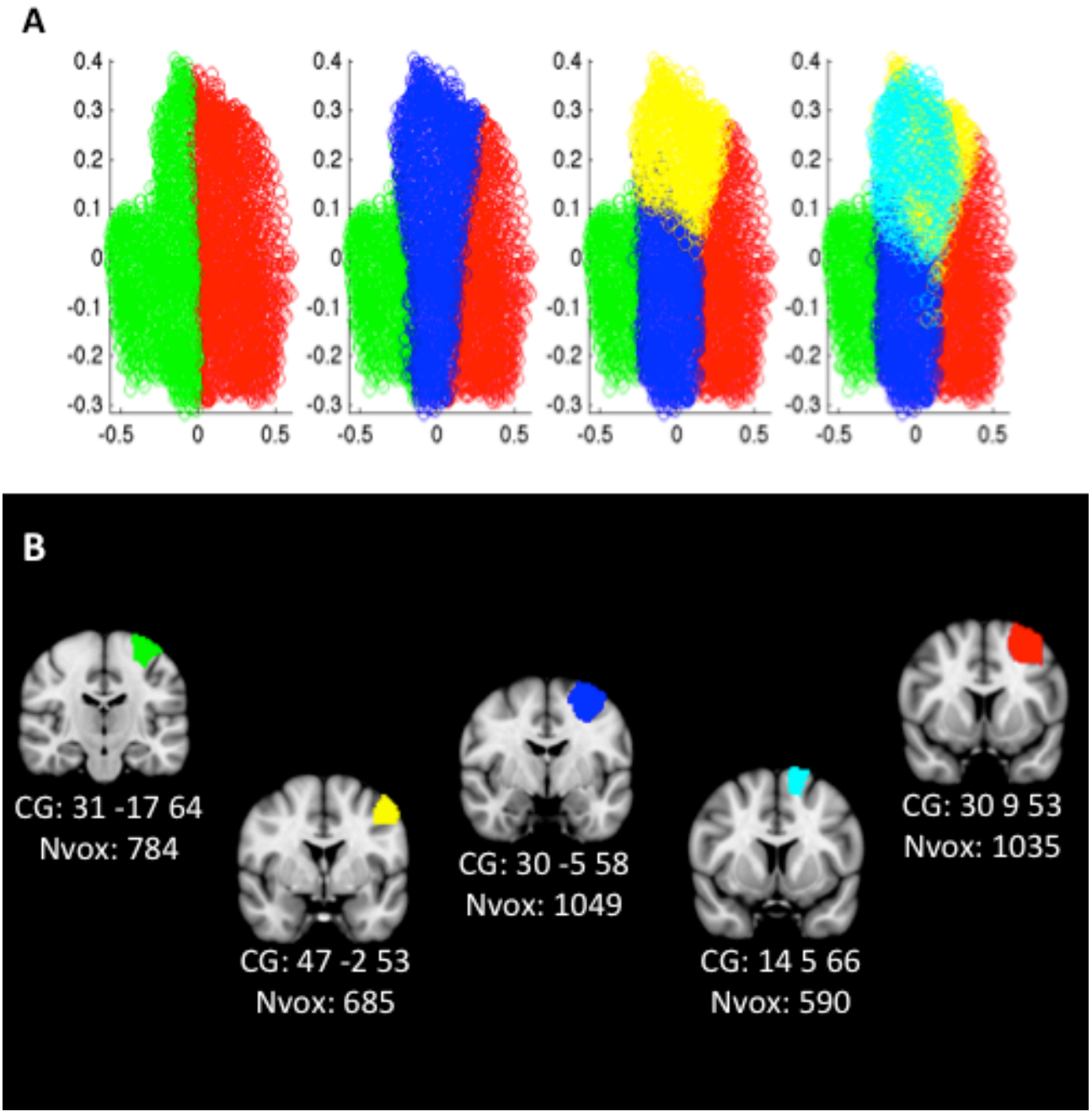
A
0.4
0.3
0.2
0.1
0
-0.1
-0.2
-0.3
-0.5
0
0.5
B
CG: 31 -17 64
Nvox: 784
CG: 47 -2 53
Nvox: 685
CG: 30 -5 58
Nvox: 1049
CG: 14 5 66
Nvox: 590
CG: 30 9 53
Nvox: 1035

Figure S4

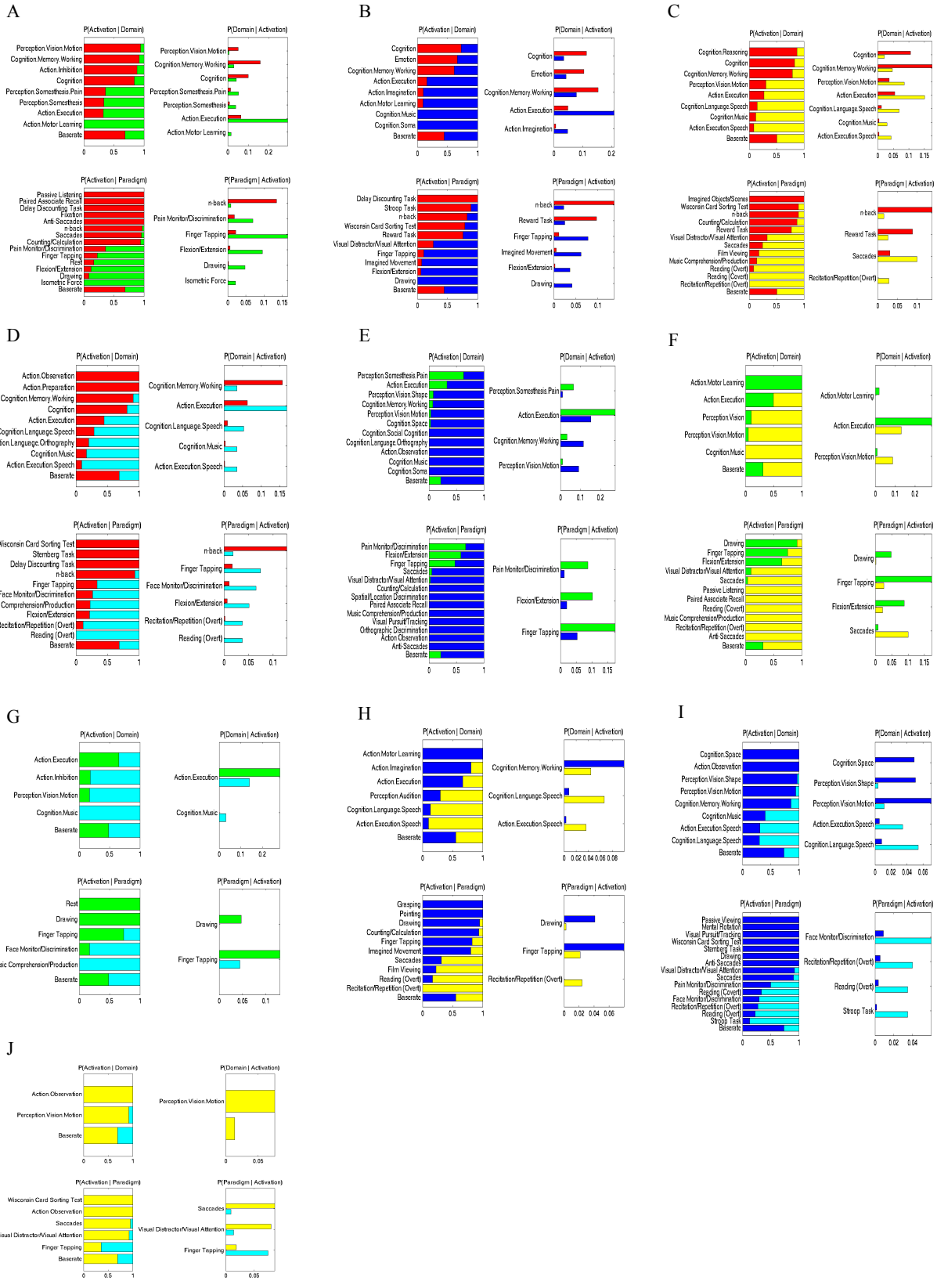
A
P(Activation | Domain)
Perception.Vision.Motion
Cognition.Memory.Working
Action.Inhibition
Cognition
Perception.Somesthesis.Pain
Perception.Somesthesis
Action.Execution
Action.Motor.Learning
Baserate
P(Domain | Activation)
Perception.Vision.Motion
Cognition.Memory.Working
Cognition
Perception.Somesthesis.Pain
Perception.Somesthesis
Action.Execution
Action.Motor.Learning
P(Activation | Paradigm)
Passive.Listening
Paired.Associate.Recall
Delay.Discounting.Task
Fixation
Anti-Saccades
n-back
Saccades
Counting/Calculation
Pain.Monitor/Discrimination
Finger.Tapping
Rest
Flexion/Extension
Drawing
Isometric.Force
Baserate
P(Paradigm | Activation)
n-back
Pain.Monitor/Discrimination
Finger.Tapping
Flexion/Extension
Drawing
Isometric.Force
B
P(Activation | Domain)
Cognition
Emotion
Cognition.Memory.Working
Action.Execution
Action.Imagination
Action.Motor.Learning
Cognition.Music
Cognition.Somesthesis
Baserate
P(Domain | Activation)
Cognition
Emotion
Cognition.Memory.Working
Action.Execution
Action.Imagination
P(Activation | Paradigm)
Delay.Discounting.Task
Stroop.Task
n-back
Wisconsin.Card.Sorting.Test
Reward.Task
Visual.Distractor/Visual.Attention
Finger.Tapping
Imagined.Movement
Flexion/Extension
Drawing
Baserate
P(Paradigm | Activation)
n-back
Reward.Task
Finger.Tapping
Imagined.Movement
Flexion/Extension
Drawing
C
P(Activation | Domain)
Cognition.Reasoning
Cognition
Cognition.Memory.Working
Perception.Vision.Motion
Action.Execution
Cognition.Language.Speech
Cognition.Music
Action.Execution.Speech
Baserate
P(Domain | Activation)
Cognition
Cognition.Memory.Working
Perception.Vision.Motion
Action.Execution
Cognition.Language.Speech
Cognition.Music
Action.Execution.Speech
P(Activation | Paradigm)
Imagined.Objects/Scenes
Wisconsin.Card.Sorting.Test
n-back
Counting/Calculation
Reward.Task
Visual.Distractor/Visual.Attention
Saccades
Film.Viewing
Music.Comprehension/Production
Reading.(Overt)
Reading.(Covert)
Recitation/Repetition.(Overt)
Baserate
P(Paradigm | Activation)
n-back
Reward.Task
Saccades
Recitation/Repetition.(Overt)
D
P(Activation | Domain)
Action.Observation
Action.Preparation
Cognition.Memory.Working
Cognition
Action.Execution
Cognition.Language.Speech
Cognition.Language.Orthography
Cognition.Music
Action.Execution.Speech
Baserate
P(Domain | Activation)
Cognition.Memory.Working
Action.Execution
Cognition.Language.Speech
Cognition.Music
Action.Execution.Speech
P(Activation | Paradigm)
Wisconsin.Card.Sorting.Test
Sternberg.Task
Delay.Discounting.Task
n-back
Finger.Tapping
Face.Monitor/Discrimination
Music.Comprehension/Production
Flexion/Extension
Recitation/Repetition.(Overt)
Reading.(Overt)
Baserate
P(Paradigm | Activation)
n-back
Finger.Tapping
Face.Monitor/Discrimination
Flexion/Extension
Recitation/Repetition.(Overt)
Reading.(Overt)
E
P(Activation | Domain)
Perception.Somesthesis.Pain
Action.Execution
Perception.Vision.Shape
Cognition.Memory.Working
Perception.Vision.Motion
Cognition.Space
Cognition.Social.Cognition
Cognition.Language.Orthography
Action.Observation
Cognition.Music
Cognition.Somesthesis
Baserate
P(Domain | Activation)
Perception.Somesthesis.Pain
Action.Execution
Cognition.Memory.Working
Perception.Vision.Motion
P(Activation | Paradigm)
Pain.Monitor/Discrimination
Flexion/Extension
Finger.Tapping
Saccades
Visual.Distractor/Visual.Attention
Counting/Calculation
Spatial/Location.Discrimination
Paired.Associate.Recall
Music.Comprehension/Production
Visual.Pursuit/Tracking
Orthographic.Discrimination
Action.Observation
Anti-Saccades
Baserate
P(Paradigm | Activation)
Pain.Monitor/Discrimination
Flexion/Extension
Finger.Tapping
F
P(Activation | Domain)
Action.Motor.Learning
Action.Execution
Perception.Vision
Perception.Vision.Motion
Cognition.Music
Baserate
P(Domain | Activation)
Action.Motor.Learning
Action.Execution
Perception.Vision.Motion
P(Activation | Paradigm)
Drawing
Finger.Tapping
Flexion/Extension
Visual.Distractor/Visual.Attention
Saccades
Passive.Listening
Paired.Associate.Recall
Reading.(Covert)
Music.Comprehension/Production
Recitation/Repetition.(Overt)
Anti-Saccades
Baserate
P(Paradigm | Activation)
Drawing
Finger.Tapping
Flexion/Extension
Saccades
G
P(Activation | Domain)
Action.Execution
Action.Inhibition
Perception.Vision.Motion
Cognition.Music
Baserate
P(Domain | Activation)
Action.Execution
Cognition.Music
P(Activation | Paradigm)
Rest
Drawing
Finger.Tapping
Face.Monitor/Discrimination
Music.Comprehension/Production
Baserate
P(Paradigm | Activation)
Drawing
Finger.Tapping
H
P(Activation | Domain)
Action.Motor.Learning
Action.Imagination
Action.Execution
Perception.Audition
Cognition.Language.Speech
Action.Execution.Speech
Baserate
P(Domain | Activation)
Cognition.Memory.Working
Cognition.Language.Speech
Action.Execution.Speech
P(Activation | Paradigm)
Grasping
Pointing
Drawing
Counting/Calculation
Finger.Tapping
Imagined.Movement
Saccades
Film.Viewing
Reading.(Overt)
Recitation/Repetition.(Overt)
Baserate
P(Paradigm | Activation)
Drawing
Finger.Tapping
Recitation/Repetition.(Overt)
I
P(Activation | Domain)
Cognition.Space
Action.Observation
Perception.Vision.Shape
Perception.Vision.Motion
Cognition.Memory.Working
Cognition.Music
Action.Execution.Speech
Cognition.Language.Speech
Baserate
P(Domain | Activation)
Cognition.Space
Perception.Vision.Shape
Perception.Vision.Motion
Action.Execution.Speech
Cognition.Language.Speech
P(Activation | Paradigm)
Passive.Viewing
Mental.Rotation
Visual.Pursuit/Tracking
Wisconsin.Card.Sorting.Test
Sternberg.Task
Drawing
Anti-Saccades
Visual.Distractor/Visual.Attention
Saccades
Pain.Monitor/Discrimination
Reading.(Covert)
Face.Monitor/Discrimination
Recitation/Repetition.(Overt)
Reading.(Overt)
Stroop.Task
Baserate
P(Paradigm | Activation)
Face.Monitor/Discrimination
Recitation/Repetition.(Overt)
Reading.(Overt)
Stroop.Task
J
P(Activation | Domain)
Action.Observation
Perception.Vision.Motion
Baserate
P(Domain | Activation)
Perception.Vision.Motion
P(Activation | Paradigm)
Wisconsin.Card.Sorting.Test
Action.Observation
Saccades
Visual.Distractor/Visual.Attention
Finger.Tapping
Baserate
P(Paradigm | Activation)
Saccades
Visual.Distractor/Visual.Attention
Finger.Tapping